Energy Reports 9 (2023) 3604–3623

Contents lists available at ScienceDirect

Energy Reports

journal homepage: www.elsevier.com/locate/egyr

Research paper

Data-driven green energy extraction: Machine learning-based MPPT control with efficient fault detection method for the hybrid PV-TEG system

Kamran Khan [a], Saad Rashid [a], Majad Mansoor [c], Ammar Khan [a], Hasan Raza [a], Muhammad Hamza Zafar [b], Naureen Akhtar [d,*]

[a] Hamdard University, Islamabad Campus, ISB 44000, Pakistan
[b] Capital University of Science and Technology, Islamabad, ISB 44000, Pakistan
[c] Department of Automation, University of Science and Technology of China, Hefei 230027, China
[d] Department of Engineering Sciences, University of Agder, Grimstad, 4876, Norway

ARTICLE INFO

Article history:
Received 14 December 2022
Received in revised form 2 February 2023
Accepted 20 February 2023
Available online 27 February 2023

Keywords:
Snake optimization (SO)
Hybrid PVTEG system
Multilayer perceptron neural network (MLPNN)
Snake optimizer based PID controller (SOPID)
Maximum power point tracking (MPPT)

ABSTRACT

The hybrid photovoltaic-thermoelectric generation system (PVTEG) gives two-fold benefits; firstly, it efficiently utilizes the available solar energy as it converts both solar irradiance and solar thermal energy into electricity, secondly, it enhances PV efficiency by reducing the PV module surface temperature. However, the efficiency of the hybrid PVTEG system is usually low because both PV and TEG are not highly efficient devices. Under changing environmental conditions, a well-designed maximum power point tracking (MPPT) controller can enhance the generation efficiency by 10%–15%. Therefore, this research explores the evolutionary Neural Network based MPPT control technique for the hybrid PVTEG systems. The snake optimizer optimally tuned weight and biases of the Multilayer perceptron neural network (MLPNN), which provides fast real-time global maxima (GM) tracking. Furthermore, to enhance the robustness of MPPT control, PID gains are tuned using the SO algorithm. Use of the snake optimizer based PID (SOPID) controller with the snake optimizer based neural network (SOANN) results in stable, accurate and fast MPPT under varying environmental conditions. The effectiveness of the proposed SOANN MPPT controller is validated by comparing it with PSOANN, RSANN and GWOANN. SOANN based MPPT controller provides very fast real-time global maxima (GM) tracking with negligible power oscillations. The SOANN controller extract optimal power with an average efficiency of 99.928% and tracking time of less than 5ms. Furthermore, an intelligent data driven based fault detection algorithm is proposed, which do not require any temperature or irradiance sensors reducing cost of the system. Comparative, simulation, quantitative, and statistical results second superior performance of SOANN controller in terms of efficiency, tracking time, stability and fault detection capability under various practical condition.

© 2023 The Author(s). Published by Elsevier Ltd. This is an open access article under the CC BY license (http://creativecommons.org/licenses/by/4.0/).

1. Introduction

The consumption of fossil fuels for energy generation is one of the main reasons for climate change. The increasing energy expenditure and the continuous dwindling of fossil fuels have diverted the attention of the power sector towards different renewable energy sources like hydroelectric, solar, wind, biogas, thermoelectric generation, etc. Renewable energy sources are preferred over traditional ones because they are theoretically unlimited, viable, highly scalable, and without pollution (Baños et al., 2011).

Solar energy is amongst the most used renewable energy sources (Zafar et al., 2021). A solar cell is used to convert solar irradiation into electrical energy. The PV cell works on the principle of photoelectric effect on the semiconductor materials. When sunlight falls on a specifically designed semiconductor solar cell, current starts flowing (Pervez et al., 2021; Moosavi et al., 2022). PV systems have multiple advantages like minimum to no operating cost, zero emissions of greenhouse gases, and low maintenance cost (Shams et al., 2021). However, PV technology also poses some drawbacks like high installation cost, low energy generation efficiency, and dependence on weather conditions (Husain et al., 2018). Another drawback of PV cells is that an increase in temperature beyond a certain level decreases the output power (Cotfas et al., 2018).

* Corresponding author.
E-mail address: naureen.akhtar@uia.no (N. Akhtar).

https://doi.org/10.1016/j.egyr.2023.02.047
2352-4847/© 2023 The Author(s). Published by Elsevier Ltd. This is an open access article under the CC BY license (http://creativecommons.org/licenses/by/4.0/).

The traditional energy generation through steam usually results in the wastage of a large amount of heat energy. A thermoelectric generator can utilize this wasted heat energy to generate electricity and this results in improved efficiency of the generation system. A thermoelectric generator operates on the principle of the See beck effect (Pourkiaei et al., 2019; Khan et al., 2022). According to this effect, when two different metals meet at one junction, voltage is produced if there is a sufficient temperature difference between the two junctions. Thermoelectric generation technology is used in military, aerospace (Jaziri et al., 2020), power generation (Elyamny et al., 2020), and wireless sensor networks. TEG is a static device with high reliability and low operational and maintenance costs. A drawback of thermoelectric generation is very low conversion efficiency as compared to the other existing renewable energy technologies (Khan et al., 2022; Aljaghtham and Celik, 2020).

The photovoltaic module transforms only a fraction of solar irradiation into electricity. Most of the valuable solar thermal energy is wasted as heat. This heat thermalize the PV cell resulting in a decrease in PV efficiency (Verma et al., 2021). An efficient scheme is required to deploy this abundant solar thermal energy. This can be achieved by the integration PV module with the TEG system (Sahin et al., 2020). The hybrid photovoltaic-thermoelectric generation system (PVTEG) gives two-fold benefits; firstly, it efficiently utilizes the available solar energy as it converts both solar insolation and solar thermal energy into electricity, secondly, it enhances PV efficiency by reducing the PV module surface temperature (He et al., 2021).

In the past, various research works explored the effectiveness of the hybrid PVTEG system. The work in Indira et al. (2020) evaluated the performance of different hybrid PVTEG models like the One-dimensional and steady-state Thermal model, One-dimensional transient thermal model, Fully Hybridized model, and Three-Dimensional model. The research study in Fathabadi (2020) proposed an improved hybrid PVTEG model. A thermosiphon heat pipe was used to increase the temperature difference. An MPPT accuracy of 96% was observed for the proposed model. The work in Shatar et al. (2018) proposed a hybrid PVTEG system for agricultural use. The integrated PVTEG provided a 3.4% increase in power when compared to the stand-alone photovoltaic system.

The efficiency of the hybrid PVTEG system is usually low because both PV and TEG are not highly efficient devices (Attivissimo et al., 2015; Gu et al., 2019; Li et al., 2018, 2014). The productivity of the hybrid PVTEG system can be increased by using new materials but it is a very cumbersome process. A simple way to boost PVTEG efficiency is to choose an appropriate MPPT technique. Under varying environmental conditions, a proper MPPT technique can increase efficiency by 15%. Therefore, an efficient MPPT algorithm is compulsory for optimizing the overall performance of the hybrid PVTEG system.

Various MPPT techniques have been explored for both TEG and PV systems (Zhang et al., 2022; Yang et al., 2019, 2020). The MPPT methods can be split up into three categories namely math-based, intelligent-based (Podder et al., 2019), and learning-based methods (Yap et al., 2020). The conventional math-based MPPT methods include: perturb and observe (Kamran et al., 2020), Hill climbing (Jately et al., 2021), ripple correlation control (Sahu and Dey, 2021) and fractional open circuit (Hmidet et al., 2021). These methods give acceptable results under uniform irradiation conditions. However, when the PV array operates under varying irradiance conditions, the traditional methods failed to track the global maximum. Various swarm intelligence-based MPPT control techniques like Improved Moth Flame (IMFO) optimization algorithm (Khan et al., 2022), Equilibrium optimization algorithm (Mansoor et al., 2021), Barnacles Mating optimization algorithm (Tariq et al., 2021), and Salp Swarm optimization algorithm (Dagal et al., 2022) are available in the literature. These meta-heuristic algorithms provide model-free optimization and have strong global search capabilities but are usually time-consuming, produce power oscillations and the search is random.

To overcome the weaknesses of the above-mentioned MPPT methods, machine learning-based methods can be used. Artificial neural networks (ANN) can efficiently handle the non-linear behavior of the hybrid PVTEG module and the uncertainty of the weather. Also, the non-linear curve fitting ability and the rapid function approximation of the neural networks make them a good choice for tracking GMPP (Fathi and Parian, 2021). However, the training of parameters such as weight & biases of the ANN is a highly complex non-convex optimization problem. Usually, deterministic methods are used for neural network training. However, these gradient-based methods have slow convergence speed, are highly dependent on initial solutions, and may trap in local minima resulting in low prediction accuracy (Khan et al., 2022; Han et al., 2019). Therefore, to overcome the shortcomings of the traditional training methods, in this work a metaheuristic Snake Optimizer (SO) (Hashim and Hussien, 2022) algorithm is used to determine the weight and biases of a multilayer perceptron neural network (MLPNN) which improves the prediction accuracy of the MLPNN. Table 1 summarizes literature review of various data driven MPPT techniques.

The literature review clearly shows that research on data driven control for a PV system is well established but there is very limited research on data driven MPPT for hybrid PVTEG systems. Most of the available research work on hybrid PVTEG system implement conventional or metaheuristic based MPPT techniques. Therefore, in this research we explored hybrid PVTEG system as an efficient energy source under varying environmental conditions by implementing the machine learning-based MPPT control.

1.1. Contributions and organization:

This paper explores the evolutionary Neural Network based MPPT control technique for the hybrid PVTEG systems, which uses a snake optimizer (SO) algorithm to train the neural network. The input dataset consists of 4 features while the output data consists of a single feature. The input features include hot junction temperature ($\boldsymbol{T_h}$), cold side temperature ($\boldsymbol{T_c}$), irradiance ($\boldsymbol{G}$), and temperature ($\boldsymbol{T}$) while reference voltage ($\boldsymbol{V_{Mpp}}$) and current ($\boldsymbol{I_{Mpp}}$) are the output features. MLPNN is trained using these input features to predict the reference voltage. This predicted voltage is given to the PID controller which generates duty cycle for the operation of the boost converter. The tuning of the PID controller requires careful handling as it might result in overshoots and static errors (Mahfoud et al., 2021). Therefore, PID gains are tuned using the SO algorithm, which enhances the robustness of the control system. Use of the SOPID controller with the SOANN algorithm results in a simple, accurate and precise MPPT controller under varying environmental conditions (see Fig. 1).

The worthy contributions of this paper are:

- A hybrid PVTEG system is explored as an efficient energy source under varying environmental conditions by implementing the machine learning-based MPPT control.
- Snake optimizer optimally tuned weight and biases of the MLPNN offline, which not only provides fast real-time GM tracking but also improves the MPPT efficiency.

Table 1
Literature review.

Reference	Technique	Summary
Kalogerakis et al. (2020)	Q-Learning based method for Global Maximum Power Point Tracking (GMPPT)	This research work uses a novel GMPPT method which implements machine learning algorithm. This method does not rely on the structure of PV modules or the operating characteristics of PV modules. The response time of this method is lesser than the traditional algorithms when subjected to random partial shading conditions. The time taken for tracking global MPPT is reduced by 80 to 98% when Q-Learning based GMPPT algorithm is applied.
Mukherjee et al. (2020)	Coarse Tree based Regression Model with and without MPPT Controller	In this work, forecasting of power generation from photovoltaic system is done by utilizing machine learning algorithm. Different models like Coarse Tree based Regression Model and Rational Quadratic Gaussian Process regression are used with and without MPPT controller for forecasting. It was observed that without MPPT controller, Coarse Tree model had the best RMSE value of 167.5 and with MPPT controller, Rational Quadratic Gaussian model had the best RMSE value of 162.8.
Padmavathi et al. (2021)	Regression Controller based MPPT	This method uses Regression Controller based MPPT in order to counter the fact that traditional methods used to change the duty cycle for MPPT like Perturb and Observe (P&O) and Particle Swarm Optimization (PSO) are greatly affected by partial shading and sudden increase in solar irradiation. The simulation and hardware results showed that for the case of strong shading, Regression controller has the best efficiency (99.78%) as compared to PSO (96.32%) and P&O (95.27%).
Phan et al. (2020)	Deep Reinforcement Learning based MPPT	This work uses two Deep Reinforcement Learning methods like the deep Q Network (DQN) and Deep Deterministic Policy Grading (DDPG) for tracking MPP in PV systems and compares its performance with traditional methods like Perturb and Observe (P&O). It was observed that not only the tracking speed of proposed methods is better but these methods can also track MPP under partial shading conditions.
Chou et al. (2019)	Reinforcement Learning based MPPT	In this paper, two reinforcement learning based methods namely Q Table MPPT and Q Network MPPT are used for MPPT tracking of photovoltaic systems. The outcomes of these techniques are compared to conventional Perturb and Observe (P&O) based MPPT. The results clearly indicate that the reinforcement learning based methods track MPP in almost 5 s as compared to P&O method which takes about 9 s for the experimental setup.
Zafar et al. (2022)	Feed-forward neural network-based Flow Direction Algorithm	In this work, Feed-forward neural network-based Flow Direction Algorithm was used to harness energy from the thermoelectric generation system. The performance of the proposed Flow Direction Algorithm was compared with particle swarm optimization (PSO), Barnacle mating optimization (BMO) and grey wolf optimization (GWO). The applied algorithm showed superior performance and achieved an efficiency of 99.89%.
Iskandar et al. (2021)	Q-Learning based with FLC	Hybrid Type-2 Fuzzy Logic Control with Q-Learning is used for MPPT of PV system under several irradiance conditions in a hybrid frame work
Gao et al. (2023)	Improved Q-learning	Divide and Conquer Q-Learning (DCQL) algorithm based Photovoltaic (PV) array reconfiguration scheme for alleviating the partial shading influence

- PID gains are tuned using the SO algorithm, which enhances the robustness of the control system. The proposed SOPID controller gives a fast transient response with no voltage oscillation.
- A novel data driven based fault detection algorithm for the hybrid PVTEG system is proposed, which do not require any temperature or irradiance sensors reducing cost of the system.

This paper consists of 5 sections. The PV and TEG modules are presented in Section 2. The explored MPPT algorithm is described in Section 3. Section 4 presents simulation results along with the statistical analysis. Finally, Section 5 concludes the paper with remarks.

2. Hybrid PVTEG system

2.1. PV modeling

The double diode model (DDM) of a PV cell is illustrated in Fig. 2. The major components of a double diode model are a current source, as PV cell basically serves as a current supplying device, two anti-parallel diodes and two resistances namely R_{sh} and R_{se}. The output current can be defined as:

$$i = i_p - i_{d1}\left(e^{\frac{V+iR_{se}}{\alpha_1 V_{T1}}} - 1\right) - i_{d2}\left(e^{\frac{V+iR_{se}}{\alpha_2 V_{T2}}} - 1\right) - \frac{V + iR_{se}}{R_{sh}} \quad (1)$$

$$i_d = (i_{SC-STC} + k_i \Delta T) \Big/ \left(e^{\left[\frac{V_{OC-STC}+k_v \Delta T}{\frac{\alpha_1+\alpha_2}{\rho}\Delta V_T}\right]-1}\right) \quad (2)$$

$$i_p = \left(i_{p-STC} + k_{i_L}(T - T_{STC})\right)\frac{G}{G_{STC}} \quad (3)$$

where i is the output current and the terminal voltage of the photovoltaic cell is represented by V, i_p is the current produced by the PV cell due to irradiance G, G_N is the irradiance at STC whereas i_{d1} and i_{d2} are the values of current at which the diode 1 and 2 saturate respectively. V_{T1} and V_{T2} are representing the values of thermal voltage constants of diodes respectively. k_i and k_v are short circuit current and open circuit voltage constants respectively. The DDM can be a single PV cell, module or array depending upon the quantity of PV cells linked in series

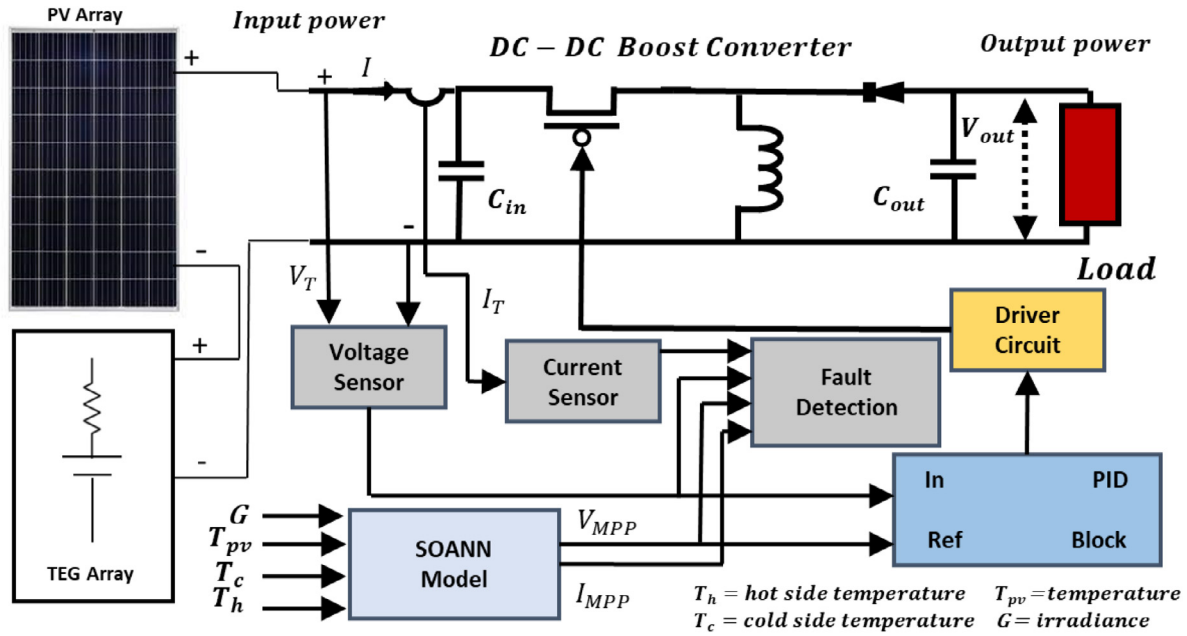

Fig. 1. SOANN based MPPT controller for hybrid PVTEG system.

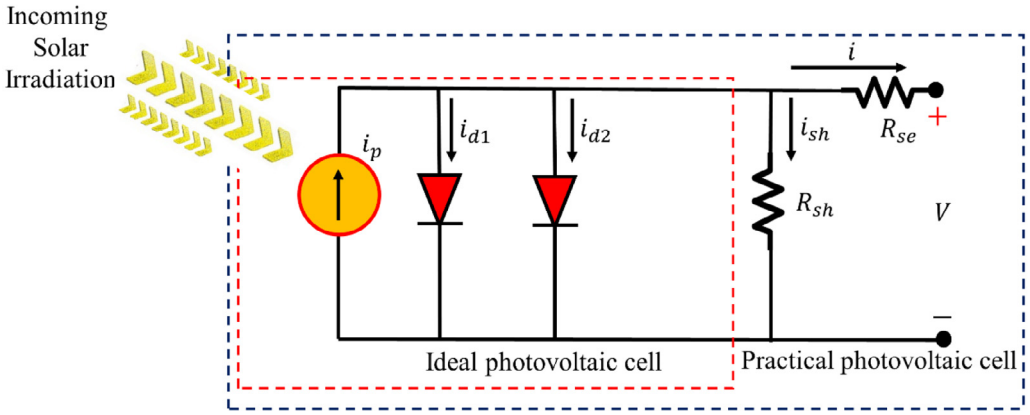

Fig. 2. Double diode model.

Table 2
PV panel (ASEC-310G6M) characteristics.

Electrical parameters	*Values*
Rated power	310.03 W
MPP voltage	35.76 V
MPP current	8.67 A
Short circuit current	9.05 A
Cells in series	72
Open circuit voltage	44.97 V
Dimension (mm)	1956 × 989 × 45

configuration m_s and parallel configuration m_p respectively (see Table 2).

$$i = m_p i_p - m_p i_{d1}\left(e^{\frac{V+\frac{m_s}{m_p}iR_{se}}{\alpha_1 m_s V_{T1}}} - 1\right) - m_p i_s\left(e^{\frac{V+\frac{m_s}{m_p}iR_{se}}{\alpha_2 m_s V_{T2}}} - 1\right) - \frac{V+\frac{m_s}{m_p}iR_{se}}{\frac{m_s}{m_p}R_{sh}} \quad (4)$$

2.2. TEG modeling

The thermoelectric generation building block consists of thermocouples which are connected in series configuration. The main objective of the thermoelectric generator is to convert thermal energy to electrical energy on the basis of Seebeck effect i.e.; the temperature difference at the junctions between two different metals results in a voltage. The electrical equivalent of a thermoelectric generator consists of a voltage source with its internal resistance. If the difference in temperature between the hot and cold junctions is constant, the open circuit voltage of a particular module is given as follows:

$$V_{TEG} = s_{p-n}\,\Delta T = s_{p-n}\,(T_h - T_c) \quad (5)$$

Where, V_{TEG} is the open circuit voltage, s_{p-n} is the Seebeck co-efficient and ΔT is the variation in temperature between the hot junction T_h and the cold junction T_c. The Seebeck co-efficient depends upon the type of the material used for TEG. The Seebeck co-efficient can be determined as follows:

$$s_{p-n} = n_t(s_p - s_n) \quad (6)$$

where n_t are the number of thermocouples, s_p and s_n indicate the Seebeck co-efficient for p-type and n-type thermocouples. The

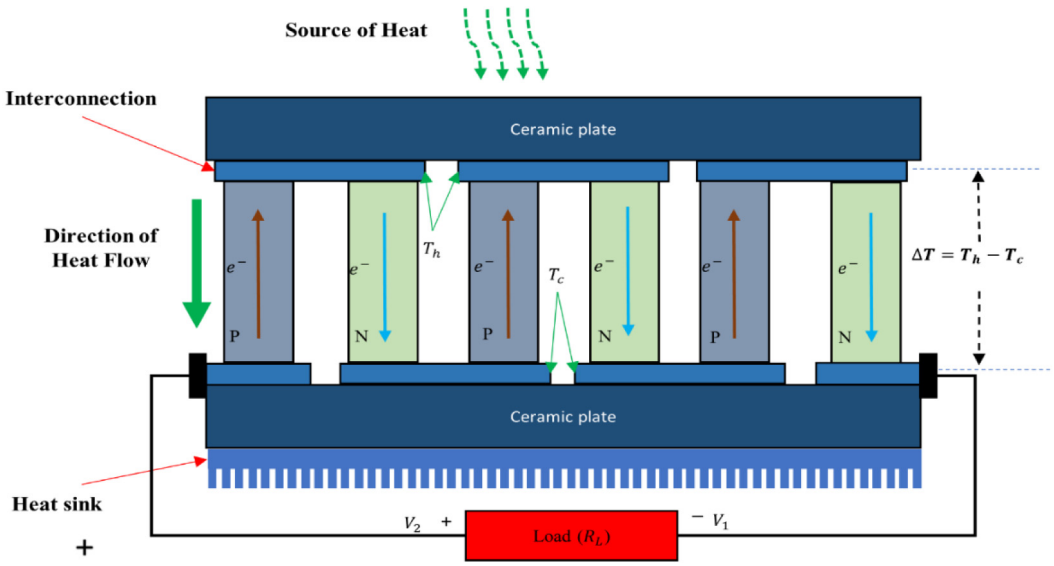

Fig. 3. TEG system.

Table 3
TEG system parameters (TE-MOD-22W7V-56).

Electrical parameters	*Values*
Resistance	1.1 Ω
Seebeck coefficient	125 μV/K
T_h (°C)	300
Parallel strings	4
T_c (°C)	30

voltage, current and output power of thermoelectric generator can be mathematically expressed as

$$V_{TEG} = \left(\frac{(s_p - s_n) \times (T_h - T_c) \times r_L}{r_L - r_{TEM}} \right) \times n_t \tag{7}$$

$$I = \frac{(s_p - s_n) \times (T_h - T_c)}{r_L - r_{TEM}} \tag{8}$$

$$P_{TEG} = r_L \times \frac{(s_p - s_n)^2 \times (T_h - T_c)^2}{(r_L - r_{TEM})^2} \times n_t \tag{9}$$

where r_L represents the load resistance in Ω and r_{TEM} represents the internal resistance of TEG (see Fig. 3 and Table 3).

2.3. PVTEG system

The integration of PV with TEG results in a highly efficient hybrid PVTEG system. The power transformation efficiency of a hybrid PVTEG system is directly proportional to the power produced by PV and TEG systems and can be mathematically represented as follows (N, 2021).

$$\eta_{pv-teg} = \frac{P_P + P_{TEG}}{G \times A_P} \tag{10}$$

where P_P = PV panel output power, P_{TEG} = TEG output power and the area of the PV panel is represented by A_P (see Fig. 4).

3. Proposed data driven MPPT controller

This research explores the evolutionary Neural Network based maximum power point tracking (MPPT) control technique for the hybrid PVTEG systems, which uses a snake optimizer (SO) algorithm to train the neural network. The MLPNN is trained using temperature of the hot junction (T_h), temperature of the cold junction (T_c), irradiance (G), and PV temperature (T) to predict the reference voltage (V_{MPP}) for maximum power extraction from the hybrid PVTEG system. The predicted V_{ref} is given to the PID controller which generates duty cycle. Furthermore, PID gains are tuned using the SO algorithm, which enhances the robustness of the control system. The SOPID controller with the SOANN algorithm results in a simple, accurate and precise MPPT controller under varying environmental conditions.

3.1. Snake Optimizer (SO)

Snake Optimization algorithm is inspired by the mating behavior of the snakes which depends upon availability of food and optimum temperature. Just like most of the optimization processes, snake optimization consists of two stages named exploration phase and exploitation phases, the exploration phase involves the exploration of search area while the exploitation phase deals with achieving the global optimum. In exploration the algorithm deals with the searching of food if it is not available nearby and eating the available food if the temperature is low i.e.; not suitable for mating while the exploitation phase deals with the mating process.

3.1.1. Mathematical model and algorithm:

The snake optimizer starts by generating a random population to start the optimization process. The population at the start of the process can be generated using the equation given below:

$$x_i = x_{min} + r \times (x_{max} - x_{min}) \tag{11}$$

where x_i is the position occupied by the ith individual, r is a randomly generated number between 0 and 1 while x_{min} and x_{max} are the lower bound and upper bound of the optimization problem.

The population is divided into two categories, males and females and the number of males and females are equal i.e.; 50%. To split the population, we use the two equations given below:

$$n_m \approx {}^{n}/_{2} \tag{12}$$

$$n_f = n - n_m \tag{13}$$

where n represents the total number of snakes, n_m represents the number of male snakes and n_f represents the number of

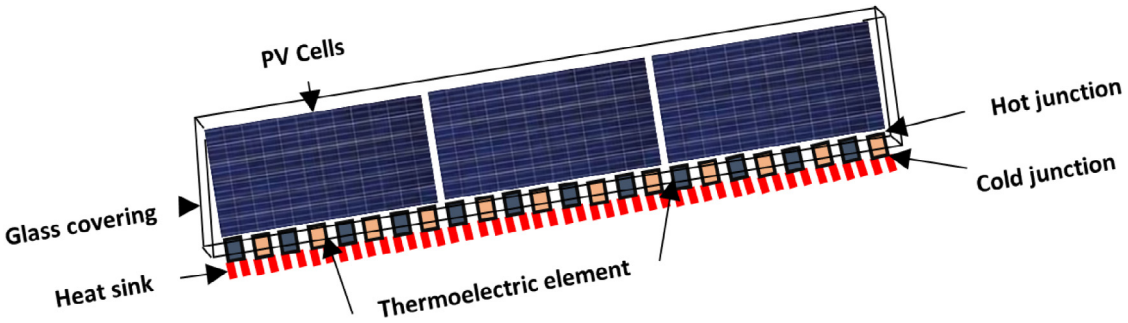

Fig. 4. Hybrid PVTEG system.

female snakes. In order to find the best individual, each group is evaluated and as a result the best male $f_{best,m}$, best female $f_{best,f}$ and the best food position f_{food} are obtained. The temperature can be described using the equation shown below:

$$Tem = e^{\frac{(-t)}{T}} \tag{14}$$

Here, t represents the value of current iteration of temperature while T represents the maximum number of iterations allowed. The food quantity can be calculated utilizing the mathematical equation given below:

$$Q = c_1 * e^{\frac{(t-T)}{T}} \tag{15}$$

where, c_1 is a constant with a value of 0.5.

3.1.2. Exploration phase

The exploration phase involves searching of food, if the food quantity is smaller than a specified threshold, the snakes start looking for food by choosing a location randomly and then update their position accordingly. The exploration phase can be modeled as follow:

$$x_{i,m}(t+1) = x_{rand,m}(t) \pm c_2 \times A_m \times ((x_{max} - x_{min}) \times rand + x_{min}) \tag{16}$$

In the above equation, $x_{i,m}$ represents the ith position of male snake, $x_{r\ and,m}$ indicates the location of the random male, *rand* is a randomly chosen number between 0 and 1, c_2 is a constant equal to 0.05 while A_m is the ability of the male snake to search for food and it can be calculated by the following relationship:

$$A_m = e^{\frac{(-f_{rand,m})}{f_{i,m}}} \tag{17}$$

Here $f_{rand,m}$ is the fitness of the $x_{rand,m}$ and $f_{i,m}$ is the fitness of individual at the ith location in the group consisting of male only.

The exploration phase for the female snakes can be modeled similar to the male snakes as follows:

$$x_{i,f} = x_{rand,f}(t+1) \pm c_2 \times A_f \times ((x_{max} - x_{min}) \times rand + x_{min}) \tag{18}$$

In this equation, $x_{i,f}$ indicates the ith female position, $x_{rand,f}$ represents the location of the random female and A_f is the capability of the female to search for food and it can be computed by the following relationship:

$$A_f = e^{\frac{(-f_{rand,f})}{f_{i,f}}} \tag{19}$$

where $f_{rand,f}$ is the fitness of $x_{rand,f}$ and $f_{i,f}$ is the fitness of the individual.

3.1.3. Exploitation phase

The exploitation phase deals with the mating process and factors effecting it. If the quantity of food is greater than the threshold and the temperature is also greater than threshold i.e.; 0.6, meaning the temperature is hot, then the only option available to the snakes will be moving towards the food. This option can be modeled mathematically as follows:

$$x_{i,j}(t+1) = x_{food} \pm c_3 \times Tem \times rand \times (x_{food} - x_{i,j}(t)) \tag{20}$$

here, $x_{i,j}$ is the location of any individual, which can either be male or female, x_{food} is the location of the best individual members of the group while c_3 is a constant whose value equals to 2.

If the temperature is colder i.e.; lower than threshold value of 0.6, then the snakes will be either in fight mode or mating mode. The fighting mode will involve two fights, there will be a fight by each male to find the best female and conversely each female to find the best male.

$$x_{i,m}(t+1) = x_{i,m}(t) \pm c_3 \times FM \times rand \times (x_{best,f} - x_{i,m}(t)) \tag{21}$$

In the above equation, $x_{i,m}$ represents ith male position, $x_{best,f}$ indicates the position of best individual in the female division and *FM* represents the fighting ability of the male agent.

$$x_{i,f}(t+1) = x_{i,f}(t+1) \pm c_3 \times FF \times rand \times (x_{best,m} - x_{i,f}(t)) \tag{22}$$

where $x_{i,f}$ represents the ith female position, $x_{best,m}$ indicates the position of the best individual in the male division and *FF* represents the fighting capability of the female agent.

We can compute the value of *FM* and *FF* as follows:

$$FM = e^{\frac{(-f_{best,f})}{f_i}} \tag{23}$$

$$FF = e^{\frac{(-f_{best,m})}{f_i}} \tag{24}$$

here, $f_{best,f}$ indicates the fitness of the best agent of the female group while $f_{best,m}$ represents the best agent in the male group and f_i is the fitness agent.

In the mating mode, start of the mating process depends upon the optimal conditions and there is a probability that the female will lay eggs that will hatch into new snakes.

$$x_{i,m}(t+1) = x_{i,m}(t) \pm c_3 \times M_m \times rand \times (Q \times x_{i,f}(t) - x_{i,m}(t)) \tag{25}$$

$$x_{i,f}(t+1) = x_{i,m}(t) \pm c_3 \times M_f \times rand \times (Q \times x_{i,m}(t) - x_{i,f}(t)) \tag{26}$$

The above two equations represent the mode of mating for male and female snakes, $x_{i,f}$ is the location of the ith individual in the female group and $x_{i,m}$ is the location of the ith individual in the male group, M_m and M_f represent the mating ability of the male and female respectively. We can collect the values of M_m and M_f as follows:

$$M_m = e^{\frac{(-f_{i,f})}{f_{i,m}}} \tag{27}$$

$$M_f = e^{\frac{(-f_{i,m})}{f_{i,f}}} \tag{28}$$

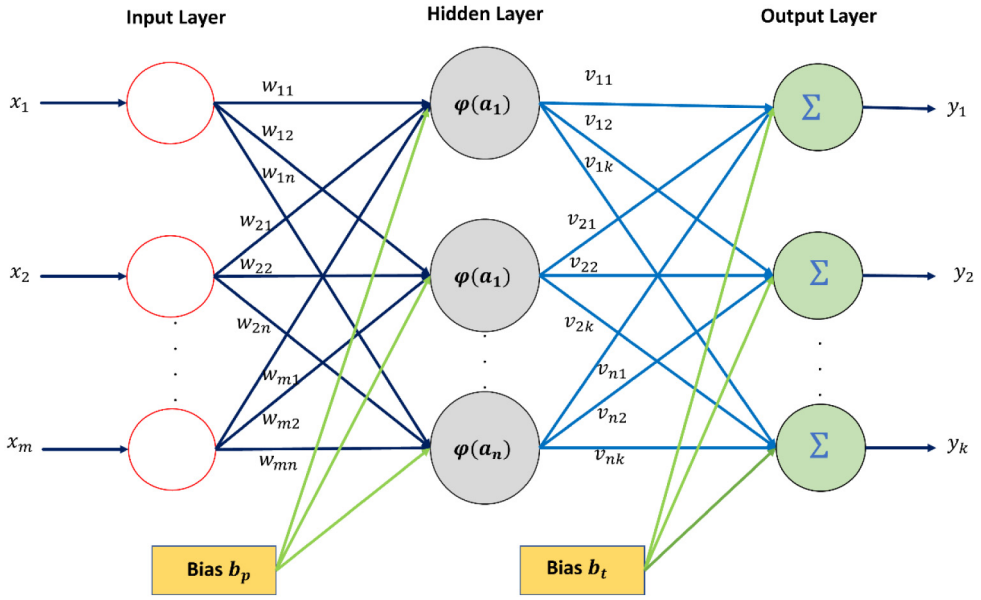

Fig. 5. Multilayer Perceptron Neural Network.

If the egg hatches, we select the worst male and female and replace them.

$$x_{worst,m} = x_{min} + rand \times (x_{max} - x_{min}) \tag{29}$$

$$x_{worst,f} = x_{min} + rand \times (x_{max} - x_{min}) \tag{30}$$

Here, $x_{worst,m}$ and $x_{worst,f}$ are the worst individual.

3.2. Trained multilayer perceptron neural network and SO tuned PID controller

3.2.1. Design of MLPNN

Artificial neural network is a machine learning technique, which computes the models based on input datasets (Naqa and Murphy, 2015). Like human brains, the artificial neural network can understand and adjust to new and changing surroundings (Jain et al., 1996). Multi-Layer Perceptron Neural Network (MLPNN) is one of the most widely used neural network models. Neurons (or nodes) are the basic elements of the MLPNN. In MLPNN neurons in a specific layer are associated with neurons available in the previous layer and each connection has a unique strength or weight as shown in Fig. 5. The neurons available in the input layer provide input to the neurons in the hidden layer and the neurons in the hidden layer act as input signals to the neurons in the output layer. Neurons existing within the same layer are not connected. The activation signal for the pth hidden layer neuron is:

$$a_p = \sum_{i=1}^{m} w_{pi}.x_i + b_p \tag{31}$$

where x_i = input vector, b_p = bias vector and w_{pi} = weight matrix. If m=input neurons and n = hidden layer neurons w_{pi} can be written as:

$$w_{pi} = \begin{bmatrix} w_{11} & w_{12} & \cdots & w_{1m} \\ w_{21} & w_{22} & \cdots & w_{2m} \\ \vdots & \vdots & \ddots & \vdots \\ w_{p1} & w_{p2} & \cdots & w_{nm} \end{bmatrix} \tag{32}$$

On the basis of the chosen activation function, the decision signal for the pth hidden layer neuron is:

$$d_p = \varphi(a_p) \tag{33}$$

For the sigmoid activation function, decision signal can be calculated as:

$$d_p = \frac{1}{1 + e^{-a_p}} \tag{34}$$

Based on these decision signal, output can be estimated by using following equation

$$y_t = \sum_{j=1}^{n} v_{tj}.d_p + b_t \tag{35}$$

Where v_{tp} = output weight matrix and b_t = output bias vector.

The purpose of training neural network is to find best weight and biases to minimize the cost function. The minimization of the cost function defines the prediction accuracy. In this study, normalized mean squared error described by Eq. (27) is used as cost function.

$$NRMSE = \frac{1}{\tilde{T}} \sqrt{\frac{1}{N} \sum_{i=1}^{N} (T_i - P_i)^2} \tag{36}$$

where T_i and p_i are the true and predicted values. $\tilde{T}$ represents the mean of true value. N represents total number of the data samples.

3.2.2. Training of MLPNN using SO

Training of parameters such as weights & biases for MLPNN is a highly complex non-convex optimization problem. Usually, deterministic methods are used for neural network training. However, these gradient-based methods suffer from slow convergence speed, are highly dependent on initial solutions, and may trap in local minima resulting in low prediction accuracy. Therefore, to overcome shortcomings of the traditional training methods, in this work metaheuristic based SO algorithm is used to determine weight and biases which not only solves most of the above-mentioned problems but also improves the prediction accuracy of the MLPNN. Fig. 6 shows the flowchart for the proposed SOANN algorithm.

The first step is dataset preparation. The dataset contains four input features and one output feature. The input features include hot side temperature, cold side temperature, irradiance, and temperature while the output feature is the reference voltage

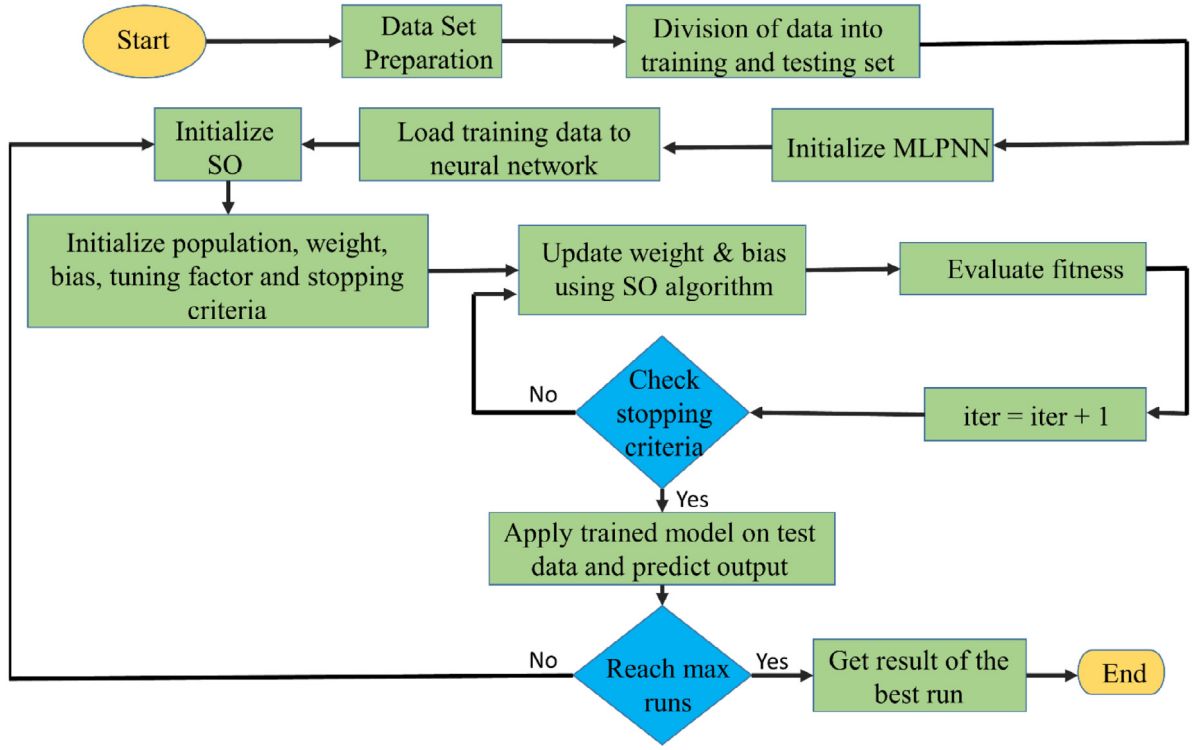

Fig. 6. Flowchart of SOANN.

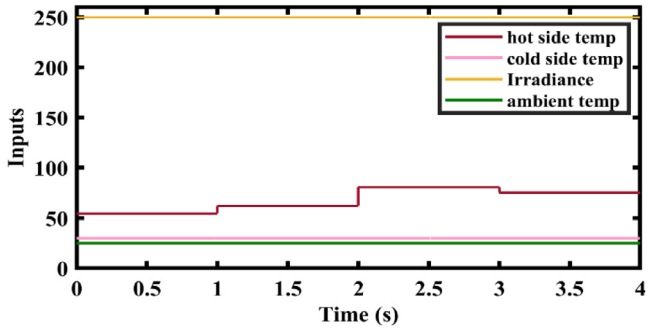

Fig. 7. Environmental conditions for case 1.

(V_{MPP}). In this research, approximately 75% of the input data is used to train the NN and the remaining 25% is used for validation purposes. After dataset preparation, the neural network is initialized with a single hidden layer. There are no fixed methods to calculate the hidden layer neurons as it is a random process. In this work, we determine the number of neurons using the formula (Faris et al., 2018).

$$s = 2 \times I + 1 \tag{37}$$

where I represents the number of input features and s shows the number of selected neurons.

After initialization, the neural network is loaded with the training data, and the SO algorithm is initialized with random weights, biases, population size, and stopping criteria. We select a population size of 50 and the algorithm stops after 50 iterations. In each iteration, weights and biases are updated using the SO algorithm and are evaluated based on the cost function. After 50 iterations, the best weights and biases are used to train the neural network. This whole process repeats 20 times. After 20 runs, the trained model with the best testing accuracy is used for the MPPT of the hybrid PVTEG system.

3.2.3. PID controller structure

The output of PID controller in time domain can be calculated by using Eq. (38)

$$u(t) = K_p e(t) + K_i \int e(t)dt + K_d \frac{de}{dt} \tag{38}$$

where K_p = proportional gain, K_i = integral gain, K_d = derivative gain. In our case error e(t) could be defined as

$$e(t) = reference\ voltage - measured\ voltage \tag{39}$$

PID controller compares the feedback measured voltage with the reference voltage predicted by ANN and produces an error signal. Based on this error the output signal (i.e., duty cycle of boost converter) is altered to make the steady state zero.

3.2.4. Snake optimizer based PID controller (SOPID)

PID controller, if not properly tuned gives undesirable overshoots, oscillations, and static errors in the nonlinear systems. Therefore, PID gains are tuned using the SO algorithm, which enhances the robustness of the control system. The tuning of the PID controller is modeled as a minimization problem with the root mean square (RMSE) as the cost function

$$RMSE = \sqrt{\frac{\sum_{t=1}^{n} \left(V_{ref} - V_{mea}\right)^2}{n}} \tag{40}$$

where V_{ref} is the reference voltage predicted by SOANN against the operating condition and V_{meas} is the output voltage at the terminal of Hybrid PVTEG system. n represents the total number of samples. In the first iteration weights are randomly initialized. In each iteration, gains are updated using the SO algorithm and are evaluated based on the cost function. After 50 iterations the best values of k_p, k_i and k_d are selected as PID gains. The tuned PID gains are $k_p = 0.016$, $k_i = 4$, and $k_d = 0$. This optimally tuned SOPID controller adjusts the operating points of hybrid PVTEG to extract optimal power by setting the duty cycle of the boost converter.

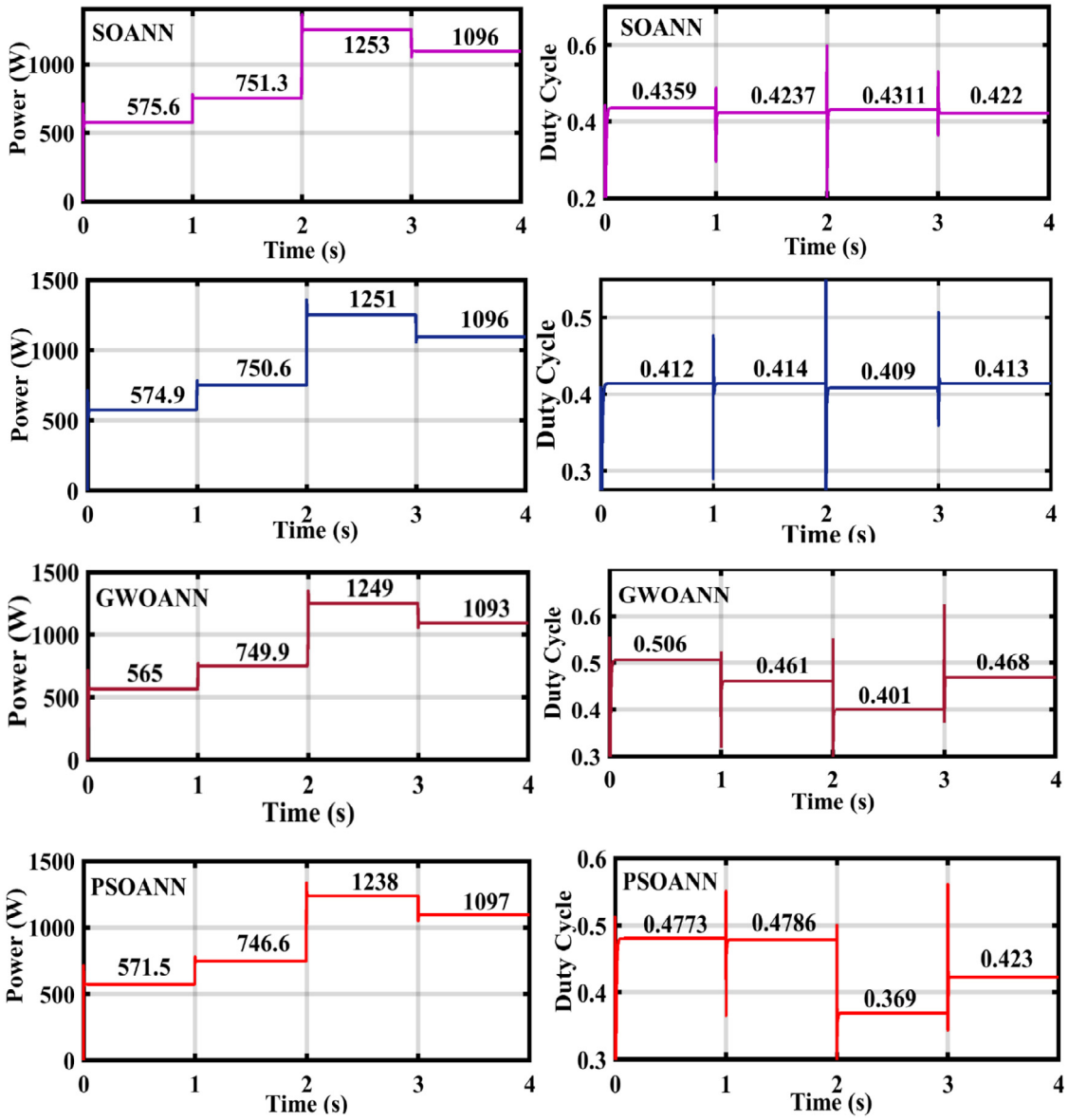

Fig. 8. Power tracking and duty cycle for Case I.

Table 4
Simulation parameters.

Component	Value
TEG Module rated power	*22* W
PV Module rated power	*310.03* W
L	*1.39* mH
C_{in}	*18* uF
C_{out}	*520* uF
Switching Frequency (f)	*50* kHz
Load	*40* Ω

4. Case studies and results:

In this section, five real-world scenarios are Simulated on a MATLAB/Simulink software considering a simulation time of 4 s. The results of the SOANN are compared with RSANN, GWOANN, and PSOANN. The first three cases determine the SOANN MPPT controller's ability to adjust to the varying atmospheric conditions like hot junction temperature gradients for TEG, cold junction temperature gradients for TEG, and irradiance variations for PV. Case 4 modeled the real-world scenario in which all the input conditions (T_h, T_c, T, G) vary at the same time while case 5 deals with the load variations. A novel fault detection mechanism is presented and tested in case 6. The simulation parameters are presented in Table 4.

4.1. Case I: Hot junction temperature (T_h) variations

In Case 1, the performance of the SOANN-based MPPT technique for a hybrid PVTEG system is evaluated by varying the hot side temperature (T_h) while keeping the other three inputs namely temperature of the cold junction, irradiation, and PV temperature constant. The variations occurred after every second. The variation in the input conditions of the hybrid PVTEG system is indicated in Fig. 7. Under given input conditions, the global maximum average power that can be extracted from a hybrid PVTEG system is 919.42 W. The average power tracked by various optimization techniques under varying input conditions is used to evaluate the effectiveness of the various MPPT techniques.

A quantitative summary of the results for case 1 is presented in Table 5. Fig. 8 indicates the variation in output power and

Table 5
Summary of results case I.

Technique	Avg predicted voltage	Avg reference voltage	Avg tracked power	Avg reference power	Energy (W s)	Efficiency (%)
SOANN	66.43	66.38	918.97	919.42	3676	99.95
RSANN	68.18	66.38	918.125	919.42	3671	99.85
GWOANN	63.15	66.38	914.225	919.42	3656	99.43
PSOANN	64.82	66.38	913.275	919.42	3653	99.33

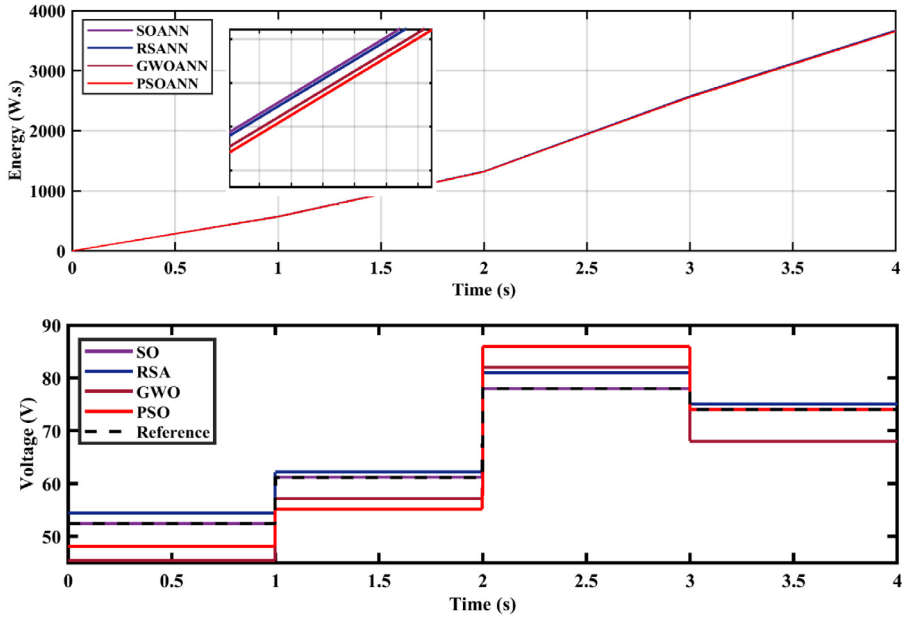

Fig. 9. (a) Extracted energy for case 1 (b) Reference and predicted voltage comparison.

duty cycle for variation in T_h. The results shows that the average power tracked by RSANN, PSOANN, GWOANN, and SOANN is 918.125 W, 913.725 W, 914.225, and 918.97 W respectively. The efficiency of the proposed SOANN is 99.95% which is higher than 99.85% of RSANN, 99.43% of GWOANN, and 99.33% of PSOANN. The comparison between the predicted voltage and the terminal voltage is another indicator to gauge the efficiency of the applied algorithms. The average voltage predicted by SOANN is 66.43 V which is closest to the actual average voltage of 66.38 V. In comparison, the voltage predicted by RSANN, GWOANN, and PSOANN is 68.18 V, 63.15 V, and 64.82 V respectively. The voltage variations are presented in Fig. 9(b). The energy extracted by various algorithms is presented in Fig. 9(a). The pictorial and quantitative results demonstrate the superior performance of the proposed SOANN algorithm.

4.2. Case II: Cold junction temperature (Tc) variations

Case II deals with the variation of cold junction temperature T_c while the temperature of the hot junction T_h, irradiation (G), and ambient temperature (T) are kept constant. For every second, the temperature of the cold junction is varied as indicated in Fig. 10. Under these given input conditions, the maximum average power that can be extracted is 1091.42 W.

Fig. 11 indicates the output power and duty cycle for different optimization techniques. From the figure, it can be seen that the average power tracked by SOANN is 1090.71 W followed by RSANN 1087.14 W, GWOANN 1074.61 W, and PSOANN 1084.72 W. The efficiency of SOANN is 99.93% which is far superior to all other optimization algorithms as indicated in Table 6. When the predicted voltage is compared with the actual voltage i.e.; 74.25 V, it can be observed that the voltage predicted by

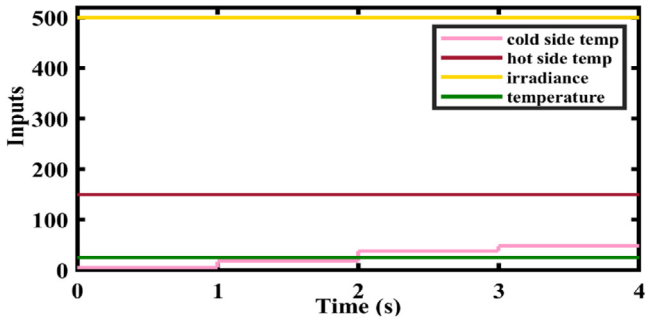

Fig. 10. Environmental conditions for case 1I.

SOANN is closest to the actual voltage i.e.; 74.43 V while the voltage predicted by RSANN is 76.37 V, GWOANN is 80.01 V and PSOANN is 77.52 V (see Fig. 12).

4.3. Case III: Irradiance (G) variations

Case III explores the variation in irradiance while keeping all other parameters constant. The variation of irradiance w.r.t time is shown in Fig. 13. The value of the average maximum power is 1042.95 W. The performance of the prosed system can be evaluated by comparing average power output of different algorithms. The Fig. 14 indicates the variation in output power and duty cycle for variation in irradiation for case III.

The average power tracked by SOANN is 1043.25 W, RSANN 1041.45 W, GWOANN 1036.32 W while PSOANN produces 1030.35 W. The efficiency of SOANN is 99.95% which is better than other algorithms. The reference voltage prediction of SOANN

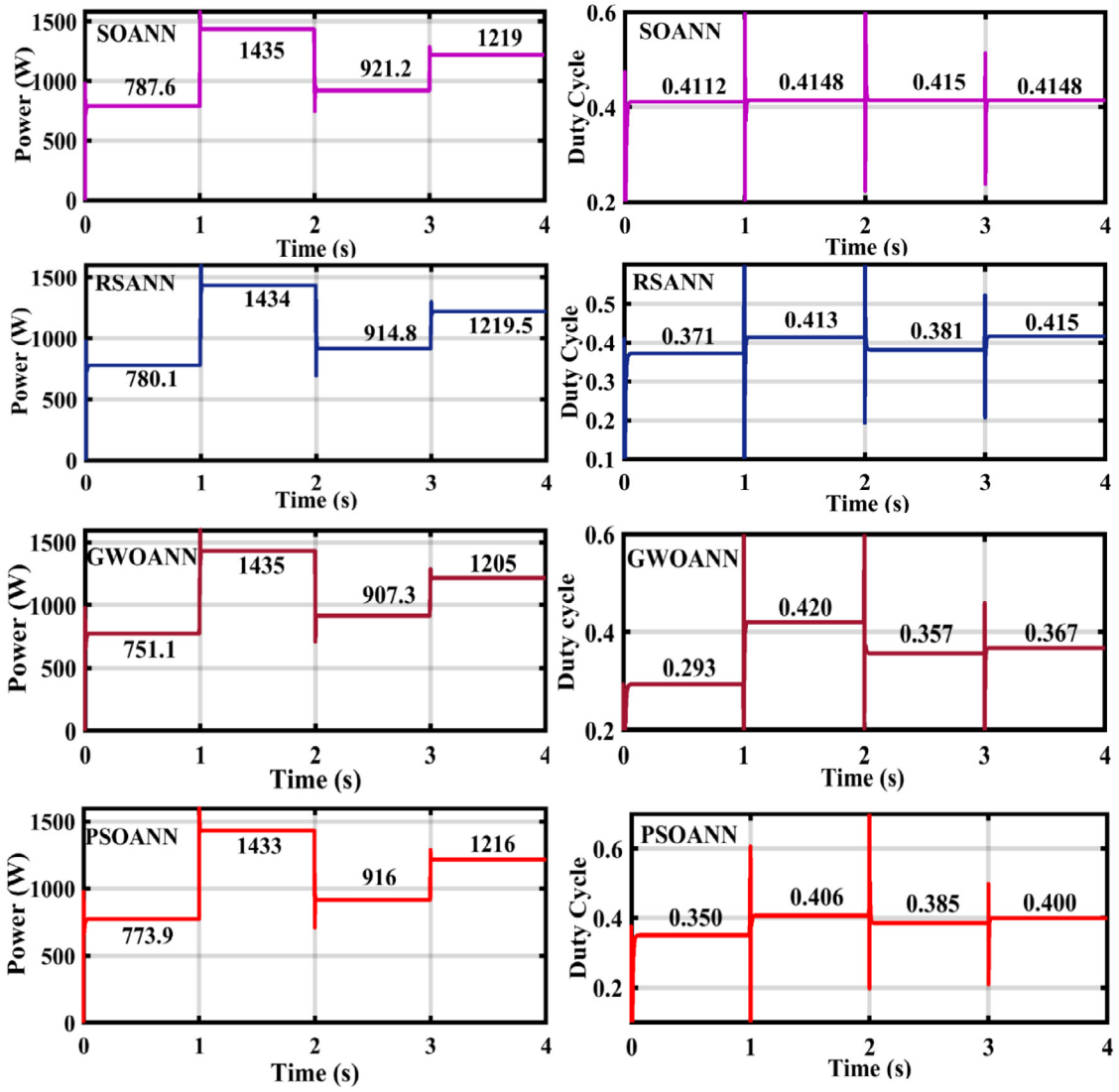

Fig. 11. Power tracking and duty cycle for Case II.

Table 6
Summary of results case II.

Technique	Avg predicted voltage	Avg reference voltage	Avg tracked power	Avg reference power	Energy (W s)	Efficiency (%)
SOANN	74.43	74.25	1090.71	1091.42	4361	99.93
RSANN	76.37	74.25	1087.14	1091.42	4347	99.60
GWOANN	80.01	74.25	1074.61	1091.42	4297	98.45
PSOANN	77.52	74.25	1084.72	1091.42	4347	99.38

Table 7
Summary of results case III.

Technique	Avg predicted voltage	Avg reference voltage	Avg tracked power	Avg reference power	Energy (W s)	Efficiency (%)
SOANN	72.99	72.24	1042.52	1042.95	4173	99.95
RSANN	74.18	72.24	1041.45	1042.95	4164	99.85
GWOANN	75.84	72.24	1036.32	1042.95	4144	99.36
PSOANN	76.97	72.24	1030.35	1042.95	4120	98.79

is 72.99 V which is closest to the actual reference voltage of 72.24 V. The comparison with other algorithms is summarized in Table 7. The energy extracted by the application of SOANN is 4173 W s which is maximum as compared to 4164 W s by RSANN, 4144 W s by GWOANN, and 4120 W s by PSOANN (see Fig. 15)

4.4. Case IV: All input parameters (T_h, T_c, G, T)

In case IV, all parameters including solar temperature (T) are varied and the effects of these variations are observed. The Fig. 16 shows variations of different parameters with respect to time (see Table 8).

Table 8
Summary of results case IV.

Technique	Avg predicted voltage	Avg reference voltage	Avg tracked power	Avg reference power	Energy (W s)	Efficiency (%)
SOANN	61.44	61.42	830.9	831.85	3322	99.88
RSANN	57.03	61.42	824.71	831.85	3299	99.14
GWOANN	54.47	61.42	819.51	831.85	3279	98.51
PSOANN	56.82	61.42	827.72	831.85	3310	99.50

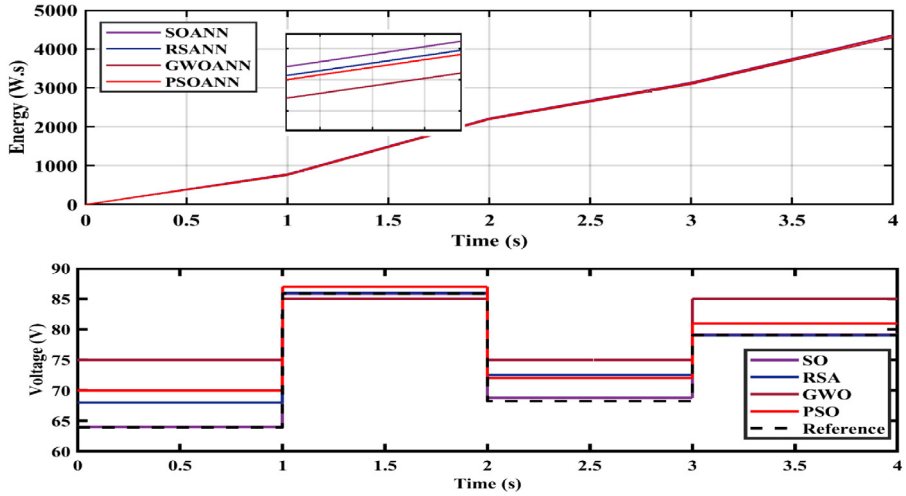

Fig. 12. (a) Extracted energy for case II (b) Reference and predicted voltage comparison.

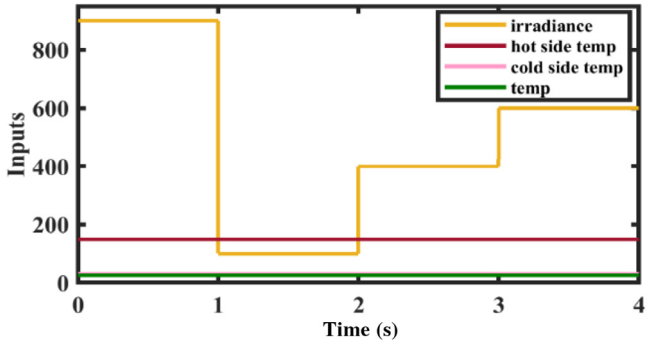

Fig. 13. Environmental conditions for case 1II.

The value of the average maximum power is 831.85 W. Power and duty cycle variations are shown in Fig. 17. The efficiency of SOANN is 99.88% which is better than 99.14% of RSANN, 98.51% of GWOANN and 99.50% of PSOANN. The reference voltage prediction of SOANN is 61.44 V which is closest to the actual reference voltage of 61.42 V as compared to 57.03 V by RSANN, 54.47 V by GWOANN and 56.82 V by PSOANN. The comparison is shown in Fig. 18(b).

From the results it can be inferred that the SOANN gives excellent results in terms of efficiency, energy extraction and voltage prediction. From Fig. 18(a) it can be seen that the energy extracted by SOANN is 3322 W s which is maximum as compared to 3299 W s by RSANN, 3279 W s by GWOANN and 3310 W s by PSOANN.

4.5. Case V: Step changes in the load

This case is modeled to simulate real-world household or commercial load variations. In real-world applications, the load can change instantly in a random manner. This behavior is emulated in this case by considering step changes in the load after every second. The load is changed from 15 to 10 and then to 5 after every second considering all the input conditions i.e., the temperature of the hot junction, the temperature of the cold junction, irradiation, and PV temperature constant. PID controller if not properly tuned may result in voltage oscillations and large overshoots at the step transitions of the load. Voltage oscillations of up to 2.8 V can be observed for the hybrid PVTEG system, which decreases the robustness of the control system. However, the proposed SOPID controller reduces voltage fluctuations and increases the safety of the equipment. Fig. 19 demonstrates the transient performance of the SOPID controller for load variations. From the figure, it can be seen that there are no oscillations and the tracking time is very small. The results demonstrate the effective transient and steady-state behavior of the SOPID controller for the dynamic variations in the load.

4.6. Case VI: Fault detection algorithm

In this case, a novel mechanism is proposed to detect abnormal or faulty behavior of the hybrid PVTEG system. To achieve maximum power, the SOANN algorithm provides two values, one is V_{MPP} and the other is I_{MPP} If output voltage V_T is equal to V_{MPP}, it means the system has reached its optimum point. In case of fault in the hybrid PVTEG system, the value of output current I_T will be somewhat lower than I_{MPP} and this difference will serve as a basis of fault detection in our system. The flowchart of the proposed fault detection mechanism is presented in Fig. 20 (see Table 9).

At the start, our system detects the output voltage of the hybrid PVTEG system after regular intervals of time namely V_{T1}, V_{T2} etc. The difference of these measured values is calculated continuously. The difference equal to zero is an indication that the system is stabilized at maximum power. The SOANN provides the optimum values of voltage and current predicted by neural network namely V_{MPP} and I_{MPP}. After the system has stabilized i.e., $\Delta V_T = 0$, the output voltage of the system V_T is then compared to the voltage predicted by neural network V_{MPP}. If the

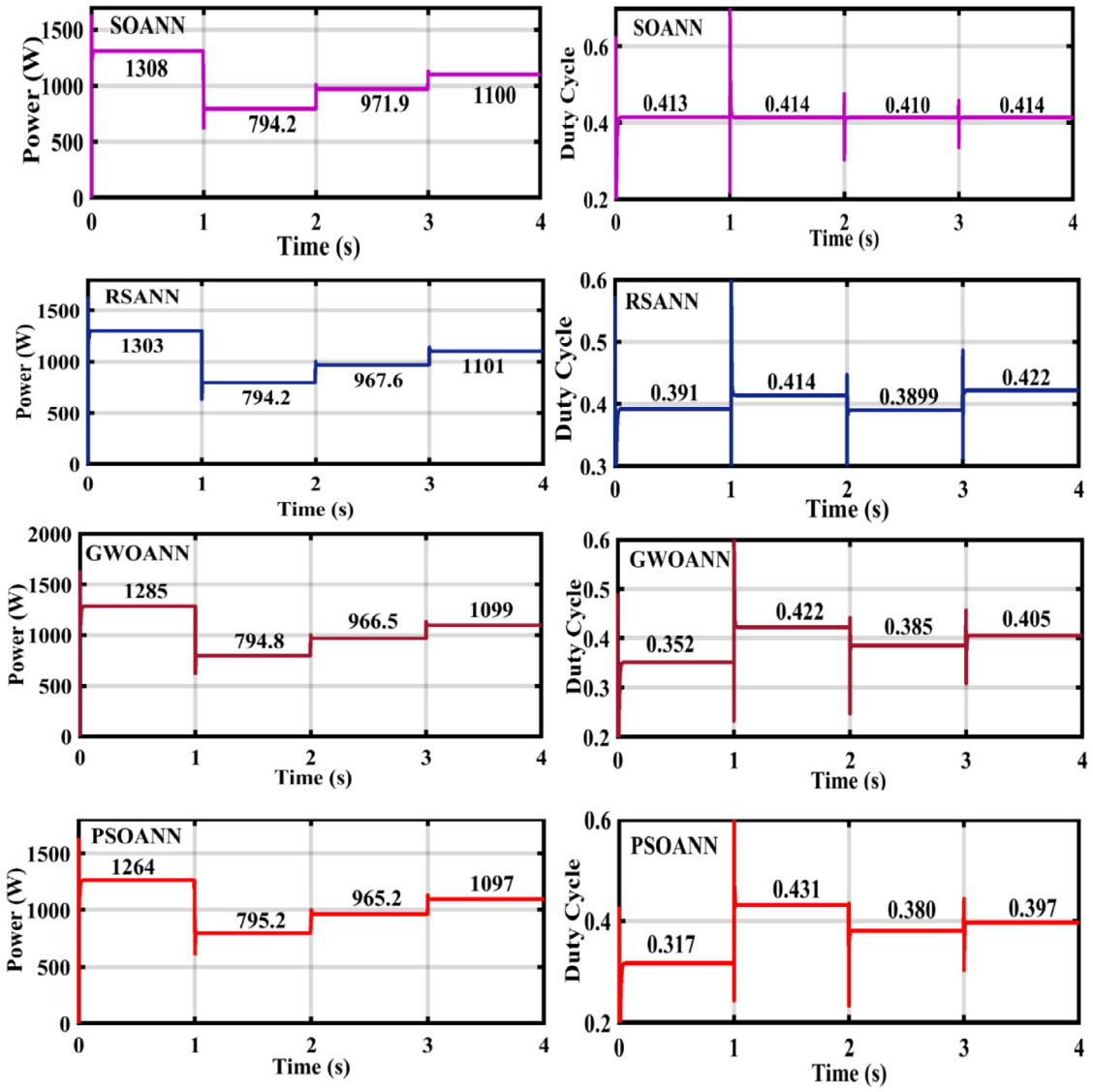

Fig. 14. Power tracking and duty cycle for Case III.

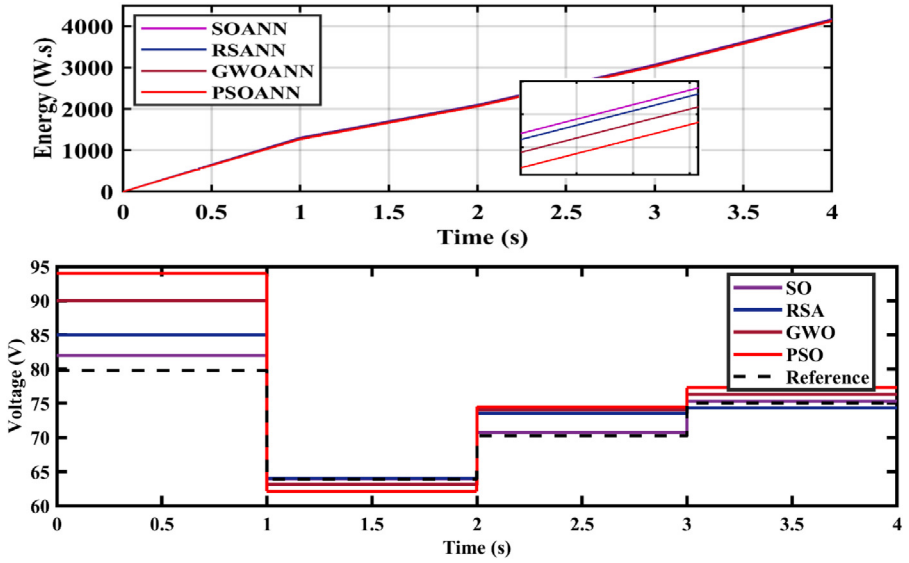

Fig. 15. (a) Extracted energy for case III (b) Reference and predicted voltage comparison.

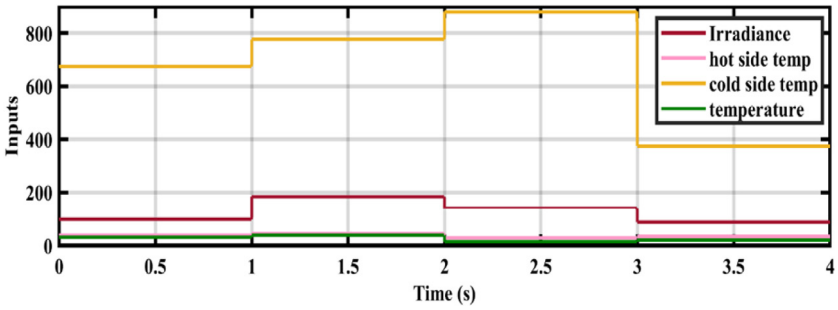

Fig. 16. Environmental conditions for case 4.

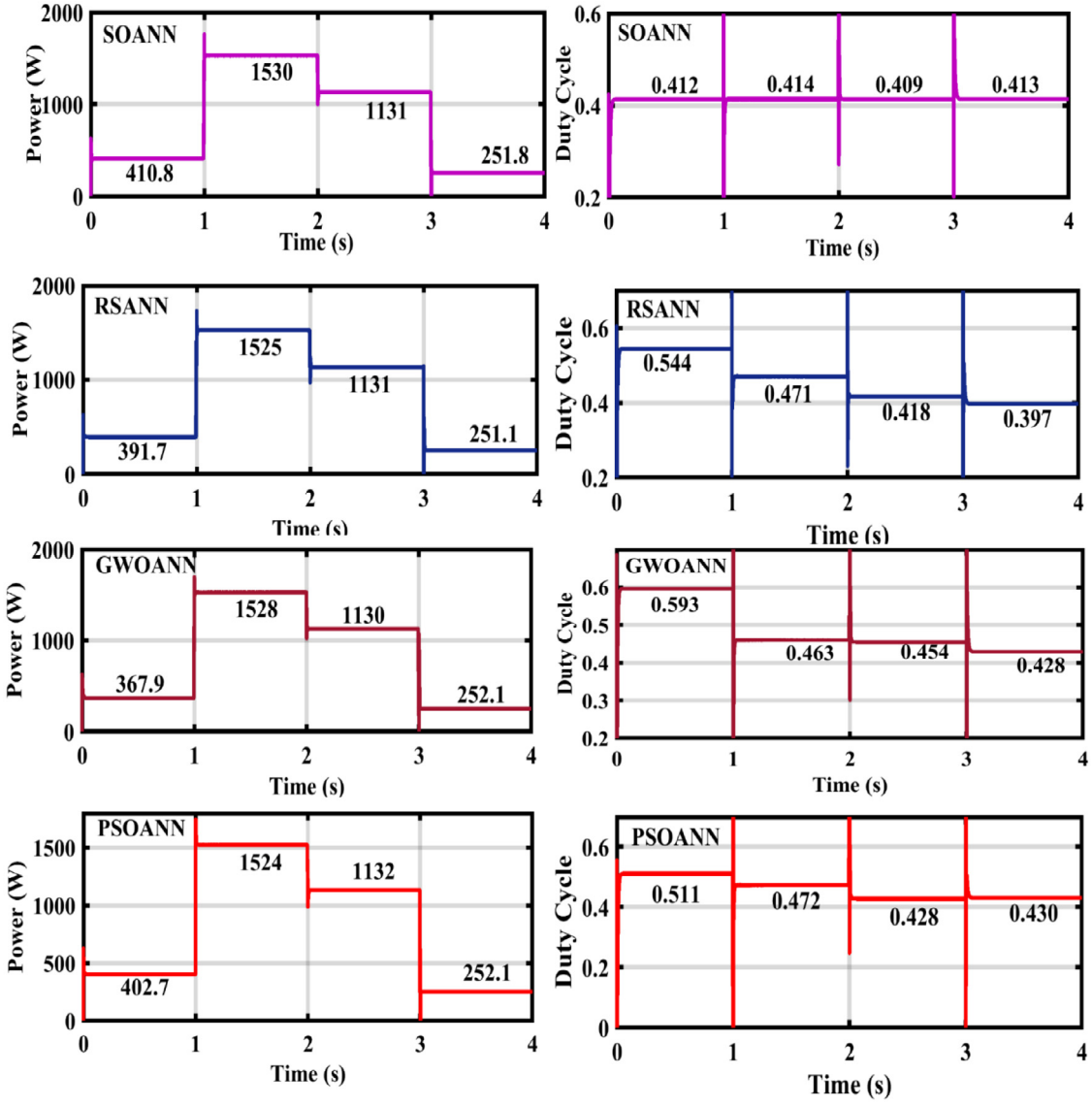

Fig. 17. Power tracking and duty cycle for Case IV.

difference of these two values is greater than a threshold level, it is a clear indication that the maximum power point tracking (MPPT) action requires some corrective measures. On the contrary, if the difference is smaller than the predefined threshold, the system output voltage is stable as well as optimum. For the detection of fault, the value of output current I_T is compared with I_{MPP} predicted by the neural network and the difference between the two values is calculated. If the difference is greater than predefined threshold, a fault is present in our system otherwise the system is stable and working perfectly. The fault detection mechanism greatly depends upon the efficiency of the neural network as well as the efficiency of the boost converter connected between the system and load. As the efficiency can never be 100%, therefore we select a threshold value of 0.5 V for voltage and 0.1 A for current. A comparison of fault current and I_{MPP} is presented in Fig. 21 (see Figs. 22, 24 and 25).

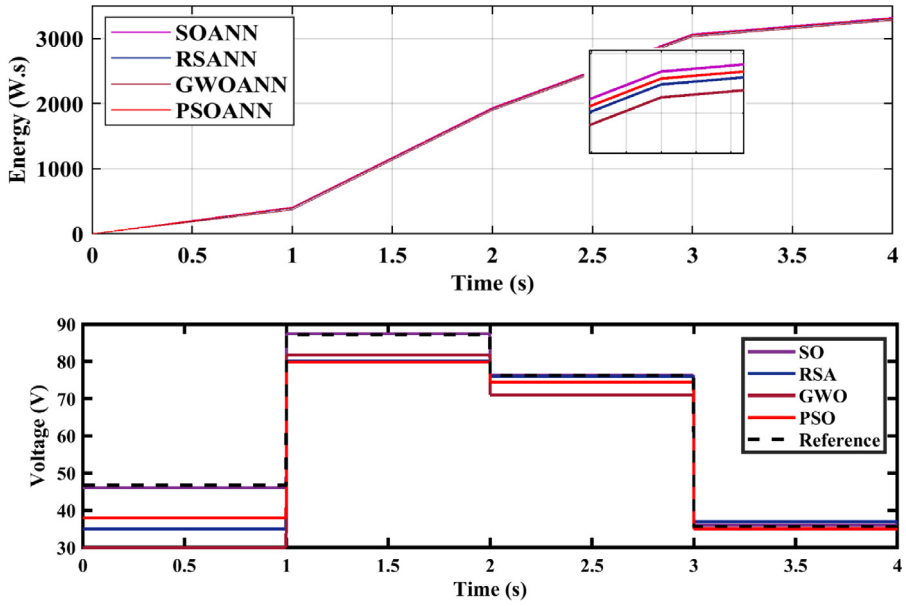

Fig. 18. (a) Extracted energy for case IV (b) Reference and predicted voltage comparison.

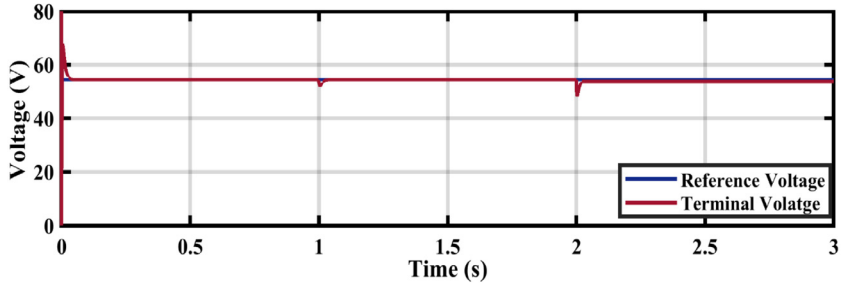

Fig. 19. SOPID controller for load variations.

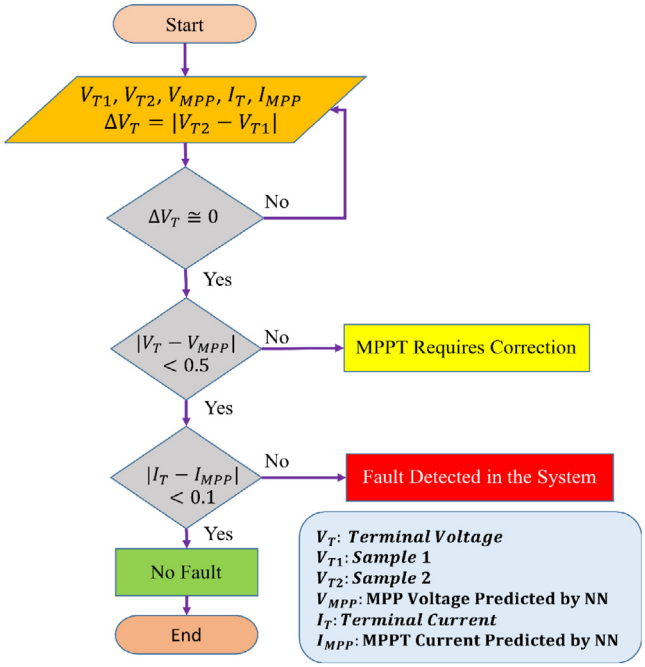

Fig. 20. Proposed Fault detection algorithm.

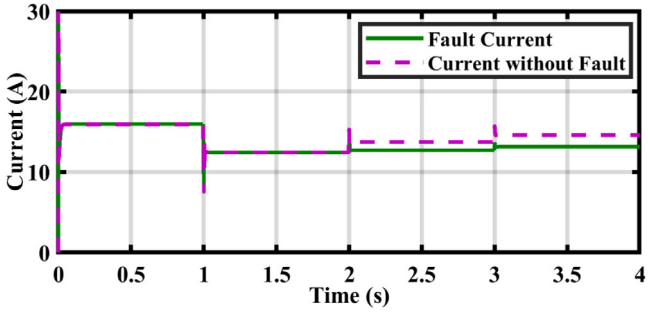

Fig. 21. Fault current and reference current.

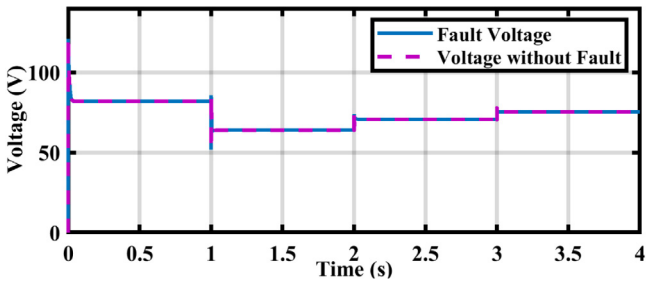

Fig. 22. Fault voltage and reference current.

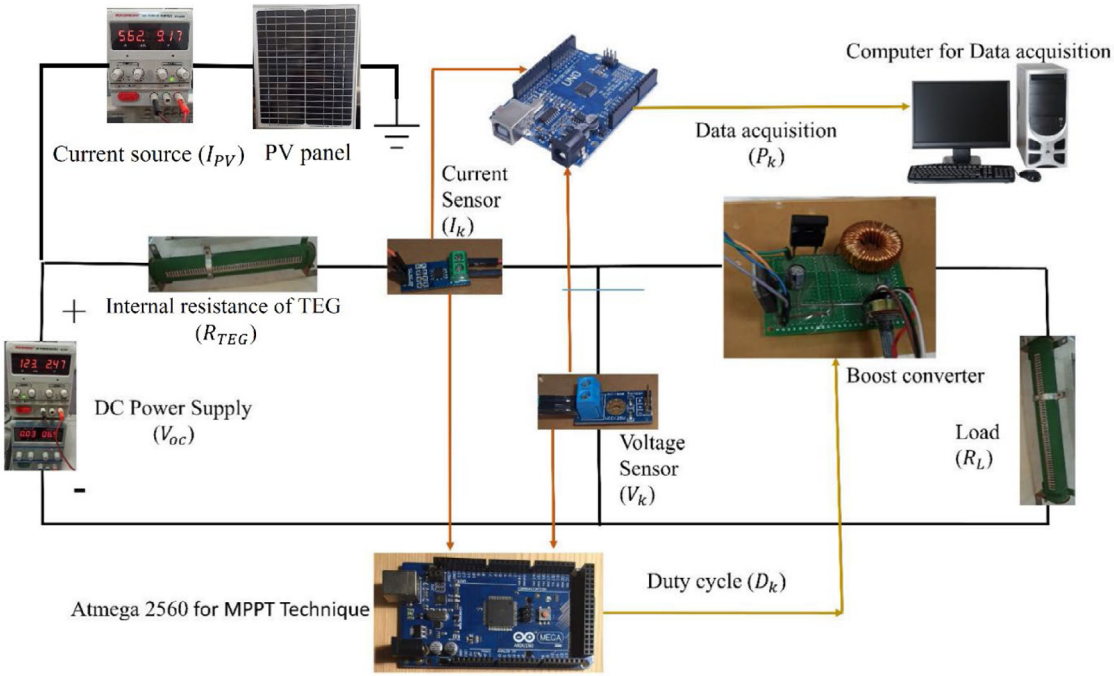

Fig. 23. PV-TEG emulator setup connections.

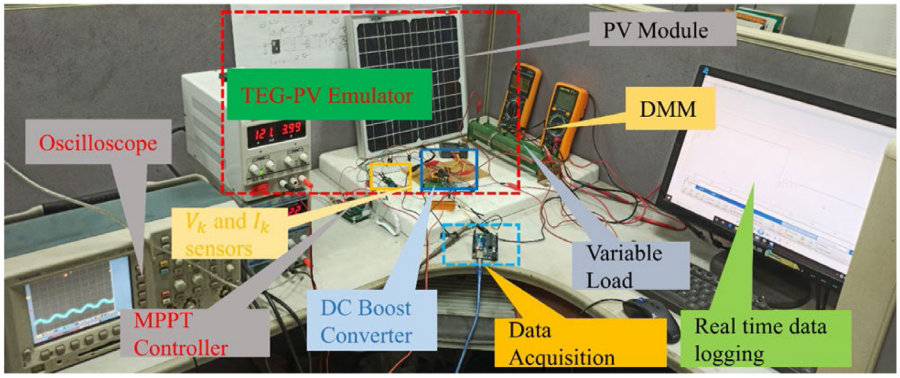

Fig. 24. PV-TEG emulator Hardware Setup.

4.7. PV-TEG emulator setup:

Realistic system model TEG acts as a voltage source with variable internal resistance (Baños et al., 2011) by operating a programmable DC voltage source as a fixed voltage-controlled voltage source the physical parameters of the TEG system can be mitigated, where the controlling voltage acts as a variation in operating temperature for the emulated TEG system using programmable DC sources with variable resistance. The objective is to mitigate the dynamic behavior of an equivalent TEG circuit where a very high temperature can be varied with precision to test the effective MPPT tracking by the proposed controller. In practice, the high temperatures can be achieved in the lab up to 250 °Cbut it causes safety issues and non-uniformity alongside relatively slower transition times. The model parameters shown in Table 10 are modeled using a datasheet provided by the manufacturer. The tolerance level provided by the manufacturer is 10%. In this study the tolerance of parameters i.e. *Voc* and *Isc* are kept well within 2% of the MPP value.

Principle: As argued in the TEG system modeling section and established through a literature survey the thermoelectric generator can be modeled as a voltage source and the internal resistance. Voltage source shows the required open-circuit voltage (V_{OC}) and internal resistance (R_{TEG}) can be modeled as a variable resistor. So, the voltage source in series with the resistance is the TEG emulator design and tested (Zafar et al., 2021). The model is verified through comprehensive analysis.

DC sweep analysis verification: The DC sweep analysis for the proposed layout of the equivalent TEG model shows a result similar to the proposed by the SAS emulator method in Pervez et al. (2021). The results confirm the behavior of the TEG is adequately emulated by this circuit. The I–V and P–V electrical characteristics performance is given by Fig. 2 as follows showing effective electrical response as of TEG module HZ-20HV at $\Delta T =$ 200 °C. SOA-FNN achieves higher power 32.2969 W as compared to GWO-FNN at 31.0094 and PSO-FNN is achieving the least power magnitude at 26.0928 W while SOA-FNN is quicker to track the power well within 160 ms as compared t o the PSO-FNN and GWO-FNN. The hardware emulator setup comparison further validates the findings of the results (see Figs. 26 and 27).

Table 9
Summary of results case VI.

Fault in module	Current difference (A)	Fault detected/Not detected
PV module-1	0.14	Detected
PV module-2	0.18	Detected
PV module-3	0.15	Detected
PV module-4	0.16	Detected
TEG module-1	0.42	Detected
TEG module-2	0.53	Detected
TEG module-3	0.33	Detected
TEG module-4	0.69	Detected

Table 10
Specifications of components used for experimental validation.

Components	Values
Oscilloscope	Tektronix TDS-3052B
Inductor(L)	1 mH
MOSFET	IRF730
Output Capacitor (C_{in})	1000 uF
Input Capacitor (C_{out})	100 uF
Micro-Controller	ATmega 2560/328
Diode	PHY 10SQ04
Load, (RL)	5,10 Ω, 300 W
Switching Frequency (f)	61 kHz
Voltage Sensor	B25 Voltage Sensor
Current Sensor module	ACS172
DC source 2	PS305 Dual channel
DC source 1	MS305-D Dual channel

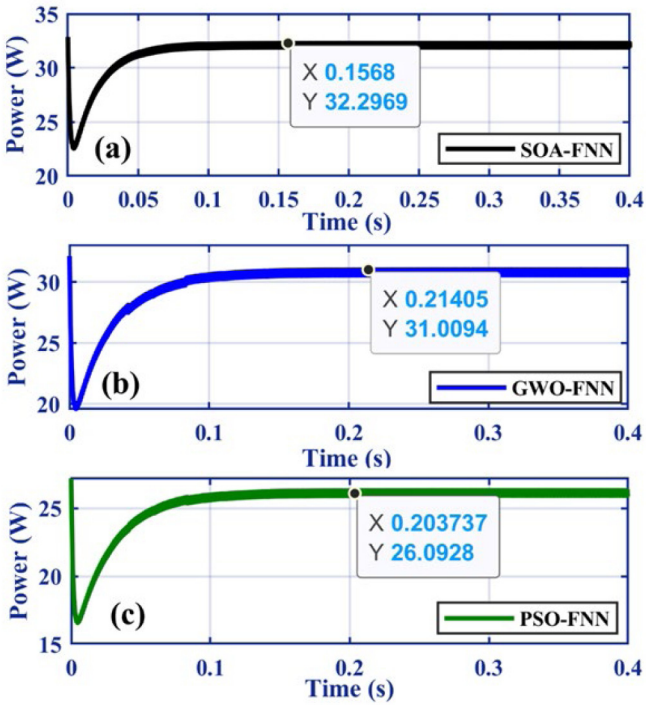

Fig. 25. Comparison of the experimental results.

4.8. Performance analysis

Metaheuristics are a type of optimization algorithm that combines both exploration and exploitation. Exploration is the process of discovering areas of the search space that may contain better solutions than the current solution. Exploitation is the process of exploiting the best solution found so far and refining it to find better solutions. To avoid local minima trapping, it is important to ensure that the search space is properly explored, the search parameters are tuned correctly, and the search procedure is suitable for the problem. The flag direction operator in the SO algorithm increases the global search capabilities. Due to this operator SO algorithm efficient explores the entire search space and avoid local minima trapping. Furthermore, Snake optimizer is easy to implement with low computational complexity and has only one tuning parameter i.e., threshold. Also, Snake Optimizer has the ability to adapt to changes in the problem it is trying to optimize, making it well suited for dynamic or non-stationary environments. Therefore, SOANN based MPPT controller provides very fast real-time global maxima (GM) tracking with negligible power oscillations. The SOANN controller gives the fastest response with an average efficiency of 99.928%. The tracking time is less than 5 ms and there are negligible oscillations around global maxima which result in low power loss and high energy output. The energy extraction by SOANN is 101.04% of the PSOANN for a simulation time of 4s. Furthermore, to enhance the robustness of MPPT control, PID gains are tuned using the SO algorithm. Tuning of PID gain by SO algorithm results in 55% faster response in comparison to the Ziegler Nicholas based PID tuning techniques. Use of the snake optimizer based PID (SOPID) controller with the snake optimizer based neural network (SOANN) results in stable, accurate and fast MPPT under varying environmental conditions.

Table 11 gives summary of results for all the considered test cases. Due to fast and stable response SOANN controller achieves 99.92% efficiency and extract highest average power and energy in comparison to RSANN, GWOANN and PSOANN. The minimization of the fitness function is another performance indicator. SOANN gives lowest cost function value of 0.134 in comparison to 0.643 by PSO.

4.9. Statistical analysis

Several statistical indicators such as the coefficient of determination (R^2), root mean square error (RMSE) and relative error (RE) can be used to evaluate the prediction proficiency of various algorithms. These indicators are described by the following equations:

$$RMSE = \sqrt{\frac{\sum_{t=1}^{n}(y_t - p_t)^2}{n}} \tag{41}$$

$$RE = \sum_{t=1}^{n}\left|\frac{y_t - p_t}{y_t}\right| \tag{42}$$

$$R^2 = 1 - \frac{\sum_{t=1}^{n}(y_t - p_t)^2}{\sum_{t=1}^{n}\left(y_t - \overline{y_j}\right)^2} \tag{43}$$

where y_t and p_t represent true and predicted values. $\overline{y_t}$ = mean value and n = number of samples.

The higher values of RE and RMSE mean poor prediction accuracy while higher value of R^2 indicate better accuracy. Table 7 describes these indicators. SOANN is ranked first in terms of accuracy as it gives the highest value of R^2 and lowest values of RMSE and RE. RSANN, GWOANN and PSOANN are ranked second, third

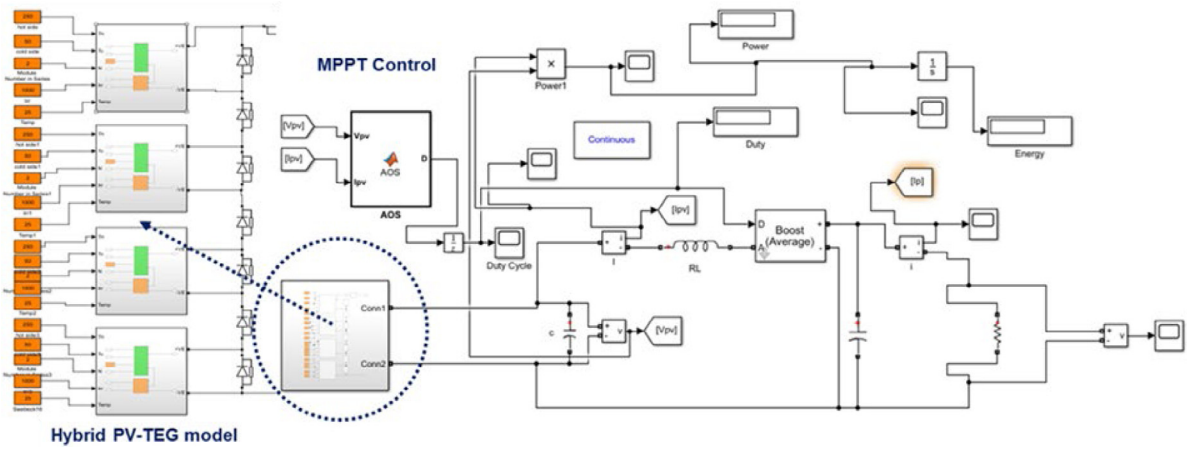

Fig. 26. Simulation setup.

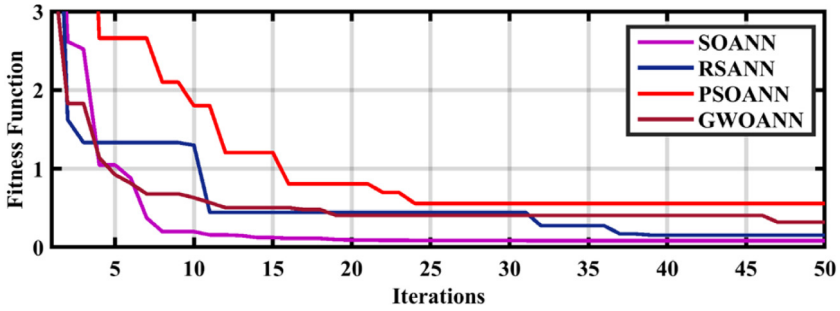

Fig. 27. Fitness function converge curve for various ANN models.

Table 11
Summary of results for considered test cases.

Technique	Avg tracked power	Avg energy extraction	Avg efficiency	Cost function
SOANN	970.77	3883.05	99.927	0.134555
RSANN	964.72	3844.12	99.43	0.170783
GWOANN	961.165	3844.66	98.93	0.301262
PSOANN	963.92	3857.71	99.25	0.64328

Table 12
Statistical indicators for various training models.

Technique	Training			Testing			Cost function
	RE	RMSE	R2	RE	RMSE	R2	
PSOANN	0.0959	32.5220	0.8278	0.2318	107.9345	0.5259	0.64328
RSANN	0.0157	11.8303	0.9835	0.0886	55.6747	0.9081	0.170783
GWOANN	0.0170	13.6071	0.9657	0.1065	61.2748	0.8890	0.301262
SOANN	0.0049	8.3396	0.9918	0.0642	32.7880	0.9665	0.134555

and fourth in terms of prediction performance. The minimization of the fitness function is another indicator of prediction accuracy. Fig. 23 shows the fitness function convergence for various training models. Table 12 shows the qualitative comparison.

5. Conclusion

Modern energy system is moving towards the era of hybrid power generation and control. To combat global warming and make the renewable cost effective the power density and efficiency of existing systems has to be improvised. One of the most cost-effective models is combination of PV and TEG that complement drawbacks of each other increasing operational efficiency of hybrid models. In this research, machine learning based SOANN MPPT controller is explored to extract maximum power from the hybrid PVTEG system and the results are compared with GWOANN, RSANN and PSOANN controllers. Simulink environment is used to study, model and analyze SOANN based Hybrid PVTEG system. The SOANN controller gives the fastest response with an average efficiency of 99.928%. The tracking time is less than 5 ms and there are negligible oscillations around global maxima which result in low power loss and high energy output. The energy extraction by SOANN is 101.04% of the PSOANN for a simulation time of 4s. Also, an intelligent and cost-effective fault detection mechanism is proposed which can efficiently detect faults in any module of the hybrid PVTEG system. Simulations, quantitative and statistical results confirms that the SOANN based controller gives fast-tracking time, high efficiency, high stability and very accurate fast detection capability.

CRediT authorship contribution statement

Kamran Khan: Conceptualization, Methodology, Resources. **Saad Rashid:** Conceptualization, Formal analysis, Investigation, Writing – review & editing. **Majad Mansoor:** Visualization, Data curation, Writing – review & editing. **Ammar Khan:** Formal analysis, Writing – review & editing. **Hasan Raza:** Investigation, Software, Writing – review & editing. **Muhammad Hamza Zafar:** Validation, Visualization, Writing – review & editing. **Naureen Akhtar:** Supervision, Project administration, Writing – review & editing.

Declaration of competing interest

The authors declare that they have no known competing financial interests or personal relationships that could have appeared to influence the work reported in this paper.

Data availability

Data will be made available on request.

References

Aljaghtham, M., Celik, E., 2020. Design optimization of oil pan thermoelectric generator to recover waste heat from internal combustion engines. Energy 200, 117547.

Attivissimo, F., et al., 2015. Feasibility of a photovoltaic–thermoelectric generator: Performance analysis and simulation results. IEEE Trans. Instrum. Meas. 64 (5), 1158–1169.

Baños, R., et al., 2011. Optimization methods applied to renewable and sustainable energy: A review. Renew. Sustain. Energy Rev. 15 (4), 1753–1766.

Chou, K.-Y., Yang, S.-T., Chen, Y.-P., 2019. Maximum power point tracking of photovoltaic system based on reinforcement learning. Sensors 19 (22), 5054.

Cotfas, D.T., Cotfas, P.A., Machidon, O.M., 2018. Study of temperature coefficients for parameters of photovoltaic cells. Int. J. Photoenergy 2018, 5945602.

Dagal, I., Akın, B., Akboy, E., 2022. Improved salp swarm algorithm based on particle swarm optimization for maximum power point tracking of optimal photovoltaic systems. Int. J. Energy Res. 46 (7), 8742–8759.

Elyamny, S., et al., 2020. High power thermoelectric generator based on vertical silicon nanowires. Nano Lett. 20 (7), 4748–4753.

Faris, H., Aljarah, I., Mirjalili, S., 2018. Improved monarch butterfly optimization for unconstrained global search and neural network training. Appl. Intell. 48 (2), 445–464.

Fathabadi, H., 2020. Novel solar-powered photovoltaic/thermoelectric hybrid power source. Renew. Energy 146, 426–434.

Fathi, M., Parian, J.A., 2021. Intelligent MPPT for photovoltaic panels using a novel fuzzy logic and artificial neural networks based on evolutionary algorithms. Energy Rep. 7, 1338–1348.

Gao, X., et al., 2023. Divide and conquer Q-learning (DCQL) algorithm based photovoltaic (PV) array reconfiguration scheme for alleviating the partial shading influence. Sol. Energy 249, 21–39.

Gu, W., et al., 2019. Mathematical modelling and performance evaluation of a hybrid photovoltaic-thermoelectric system. Energy Convers. Manage. 198, 111800.

Han, F., et al., 2019. A survey on metaheuristic optimization for random single-hidden layer feedforward neural network. Neurocomputing 335, 261–273.

Hashim, F.A., Hussien, A.G., 2022. Snake optimizer: A novel meta-heuristic optimization algorithm. Knowl.-Based Syst. 242, 108320.

He, Z., et al., 2021. Concentrated photovoltaic thermoelectric hybrid system: an experimental and machine learning study. Engineered Sci. 15, 47–56.

Hmidet, A., et al., 2021. Design of efficient off-grid solar photovoltaic water pumping system based on improved fractional open circuit voltage MPPT technique. Int. J. Photoenergy 2021, 4925433.

Husain, A.A.F., et al., 2018. A review of transparent solar photovoltaic technologies. Renew. Sustain. Energy Rev. 94, 779–791.

Indira, S.S., et al., 2020. A review on various configurations of hybrid concentrator photovoltaic and thermoelectric generator system. Sol. Energy 201, 122–148.

Iskandar, R.F., Leksono, E., Joelianto, E., 2021. Q-learning hybrid type-2 fuzzy logic control approach for photovoltaic maximum power point tracking under varying solar irradiation exposure. Int. J. Intell. Eng. Syst. 15, 199–208.

Jain, A.K., Jianchang, M., Mohiuddin, K.M., 1996. Artificial neural networks: A tutorial. Computer 29 (3), 31–44.

Jately, V., et al., 2021. Experimental analysis of hill-climbing MPPT algorithms under low irradiance levels. Renew. Sustain. Energy Rev. 150, 111467.

Jaziri, N., et al., 2020. A comprehensive review of thermoelectric generators: Technologies and common applications. Energy Rep. 6, 264–287.

Kalogerakis, C., Koutroulis, E., Lagoudakis, M.G., 2020. Global MPPT based on machine-learning for PV arrays operating under partial shading conditions. Appl. Sci. 10 (2), 700.

Kamran, M., et al., 2020. Implementation of improved perturb & observe MPPT technique with confined search space for standalone photovoltaic system. J. King Saud Univ., Eng. Sci. 32 (7), 432–441.

Khan, N.M., et al., 2022. Energy harvesting and stability analysis of centralized TEG system under non-uniform temperature distribution. Sustain. Energy Technol. Assess. 52, 102028.

Li, Y., et al., 2014. Wide spectrum solar energy harvesting through an integrated photovoltaic and thermoelectric system. Particuology 15, 39–44.

Li, G., et al., 2018. A review of solar photovoltaic-thermoelectric hybrid system for electricity generation. Energy 158, 41–58.

Mahfoud, S., et al., 2021. A new strategy-based PID controller optimized by genetic algorithm for DTC of the doubly fed induction motor. Systems 9 (2), 37.

Mansoor, M., et al., 2021. Maximum energy harvesting of centralized thermoelectric power generation systems with non-uniform temperature distribution based on novel equilibrium optimizer. Energy Convers. Manage. 246, 114694.

Moosavi, S.K.R., et al., 2022. Highly efficient maximum power point tracking control technique for PV system under dynamic operating conditions. Energy Rep. 8, 13529–13543.

Mukherjee, D., et al., 2020. Machine learning based solar power generation forecasting with and without MPPT controller. In: 2020 IEEE 1st International Conference for Convergence in Engineering. ICCE.

N, K., 2021. Photovoltaic and thermoelectric generator combined hybrid energy system with an enhanced maximum power point tracking technique for higher energy conversion efficiency. Sustainability 13 (6), 3144.

Naqa, I.El., Murphy, M.J., 2015. What is machine learning? In: Naqa, I. El, Li, R., Murphy, M.J. (Eds.), Machine Learning in Radiation Oncology: Theory and Applications. Springer International Publishing, Cham, pp. 3–11.

Padmavathi, N., Chilambuchelvan, A., Shanker, N.R., 2021. Maximum power point tracking during partial shading effect in PV system using machine learning regression controller. J. Electr. Eng. Technol. 16 (2), 737–748.

Pervez, I., et al., 2021. Most valuable player algorithm based maximum power point tracking for a partially shaded PV generation system. IEEE Trans. Sustain. Energy 12 (4), 1876–1890.

Phan, B.C., Lai, Y.-C., Lin, C.E., 2020. A deep reinforcement learning-based MPPT control for PV systems under partial shading condition. Sensors 20 (11), 3039.

Podder, A.K., Roy, N.K., Pota, H.R., 2019. MPPT methods for solar PV systems: A critical review based on tracking nature. IET Renew. Power Gener. 13 (10), 1615–1632.

Pourkiaei, S.M., et al., 2019. Thermoelectric cooler and thermoelectric generator devices: A review of present and potential applications, modeling and materials. Energy 186, 115849.

Sahin, A.Z., et al., 2020. A review on the performance of photovoltaic/thermoelectric hybrid generators. Int. J. Energy Res. 44 (5), 3365–3394.

Sahu, P., Dey, R., 2021. Maximum power point tracking for photovoltaic systems using ripple correlation control. In: 2021 International Conference on Control, Automation, Power and Signal Processing. CAPS.

Shams, I., Mekhilef, S., Tey, K.S., 2021. Maximum power point tracking using modified butterfly optimization algorithm for partial shading, uniform shading, and fast varying load conditions. IEEE Trans. Power Electron. 36 (5), 5569–5581.

Shatar, N.M., et al., 2018. Design of photovoltaic-thermoelectric generator (PV-TEG) hybrid system for precision agriculture. In: 2018 IEEE 7th International Conference on Power and Energy. PECon.

Tariq, M.I., et al., 2021. Optimal control of centralized thermoelectric generation system under nonuniform temperature distribution using barnacles mating optimization algorithm. Electronics 10. http://dx.doi.org/10.3390/electronics10222839.

Verma, S., et al., 2021. Cooling techniques of the PV module: A review. Mater. Today: Proc. 38, 253–258.

Yang, B., et al., 2019. MPPT design of centralized thermoelectric generation system using adaptive compass search under non-uniform temperature distribution condition. Energy Convers. Manage. 199, 111991.

Yang, B., et al., 2020. Comprehensive overview of maximum power point tracking algorithms of PV systems under partial shading condition. J. Clean. Prod. 268, 121983.

Yap, K.Y., Sarimuthu, C.R., Lim, J.M.Y., 2020. Artificial intelligence based MPPT techniques for solar power system: A review. J. Mod. Power Syst. Clean Energy 8 (6), 1043–1059.

Zafar, M.H., et al., 2021. Bio-inspired optimization algorithms based maximum power point tracking technique for photovoltaic systems under partial shading and complex partial shading conditions. J. Clean. Prod. 309, 127279.

Zafar, M.H., et al., 2022. Towards green energy for sustainable development: Machine learning based MPPT approach for thermoelectric generator. J. Clean. Prod. 351, 131591.

Zhang, R., Yang, B., Chen, N., 2022. Arithmetic optimization algorithm based MPPT technique for centralized TEG systems under different temperature gradients. Energy Rep. 8, 2424–2433.